arXiv:0805.3067v1 [hep-ph] 20 May 2008

Single-top hadroproduction in association with a W boson

Stefano Frixione[*]

> *PH Department, TH Unit, CERN, CH-1211 Geneva 23, Switzerland*
> *ITPP, EPFL, CH-1015 Lausanne, Switzerland*
> *E-mail:* Stefano.Frixione@cern.ch

Eric Laenen

> *ITFA, University of Amsterdam, Valckenierstraat 65, 1018 XE Amsterdam,*
> *Nikhef Theory Group, Kruislaan 409, 1098 SJ Amsterdam, The Netherlands*
> *ITF, Utrecht University, Leuvenlaan 4, 3584 CE Utrecht*
> *E-mail:* Eric.Laenen@nikhef.nl

Patrick Motylinski

> *Nikhef Theory Group, Kruislaan 409, 1098 SJ Amsterdam, The Netherlands*
> *E-mail:* patrickm@nikhef.nl

Bryan R. Webber

> *Cavendish Laboratory, J.J. Thomson Avenue, Cambridge CB3 0HE, U.K.*
> *E-mail:* webber@hep.phy.cam.ac.uk

Chris White

> *Nikhef Theory Group, Kruislaan 409, 1098 SJ Amsterdam, The Netherlands*
> *E-mail:* cwhite@nikhef.nl

ABSTRACT: We present the calculation of the Wt single-top production channel to next-to-leading order in QCD, interfaced with parton showers within the MC@NLO formalism. This channel provides a complementary way of investigating the properties of the Wtb vertex, with respect to the s- and t-channels. We pay special attention to the separation of this process from top quark pair production.

---

[*]On leave of absence from INFN, Sez. di Genova, Italy

Contents

1. Introduction

The top quark was discovered in 1995 and has been intensively studied at the Tevatron. It will also be a prime object of study at the forthcoming Large Hadron Collider (LHC). With production rates far in excess of current experiments, the LHC can be thought of as a veritable top quark factory. The large mass of the quark, near the electroweak scale, enables detailed scrutiny of its interactions unshrouded by hadronisation effects (which are suppressed by powers of the perturbative momentum scale). Furthermore, effects of physics beyond the Standard Model are thought to lie around

the electroweak scale, thus the top quark sector provides a valuable window for new physics.

A useful process to study in this regard is the production of single top quarks via the weak interaction, as it offers a relatively clean probe of the properties of the heavy quark. Although there was recently at least a 3σ evidence of single top production at both Tevatron experiments (see e.g. refs. [1, 2]), the cross section is sufficiently small (within the SM) as to preclude detailed scrutiny. However, one expects a significant number of single top events at the LHC, where the centre of mass energy is much higher.

Accurate estimates of rates and kinematic distributions at hadron colliders necessitate higher-order perturbative computations in QCD. Furthermore, in order to optimise acceptance cuts in experimental analyses or perform full detector simulations, one needs realistic hadron-level events. These are obtained using Monte Carlo event generators that incorporate the simulation of parton showers and hadronisation models. The complementary benefits of fixed-order computations and parton shower simulations are by now well-known, as are the advantages of combining them into a framework which utilizes the benefits of each of them. The MC@NLO approach [3, 4] provides a way of achieving this, by allowing one to match cross sections computed at NLO in QCD with an event generator. No modifications to the latter are necessary, and colour coherence is preserved by the matching procedure. Therefore, existing parton shower Monte Carlos with no add-ons can be used for this purpose.

There are three distinct production modes for single top quarks. In earlier work [5] we included two of these modes, the s- and t-channel processes, into the MC@NLO framework. In this paper, we implement the production of a single top quark in association with a final state W boson, thereby completing the description of single top processes in hadronic collisions at this level of accuracy, including spin correlations of decay products, which we incorporate as explained in ref. [6].

As is well known, the inclusion of higher order corrections for the Wt channel has challenging peculiarities due to interference with the $t\bar{t}$ process. This interference becomes extremely large in certain phase-space regions, and apparently renders the perturbative computation of the Wt cross section meaningless. Nevertheless, owing to distinct features of $t\bar{t}$ production, several *definitions* of the Wt channel have been given in the literature, each with the aim of recovering a well-behaved expansion in α_{s}. The problem of interference in fact affects any computation that considers contributions beyond the leading order, i.e. at least $\mathcal{O}(g_{\mathrm{w}}^2\alpha_{\mathrm{s}}^2)$. The cross section at this order has been previously presented in refs. [7, 8, 9], where only tree-level graphs were considered, and in refs. [10, 11, 12], where one-loop contributions were included as well. In ref. [13], the calculation of NLO electroweak effects has been carried out, using the results of ref. [11] as a basis. We shall comment on some of these papers in the following.

The aim of this paper is to critically examine the definition of the Wt channel,

and to propose two options that can be used in the context of an NLO calculation interfaced with parton showers. Although these two options are well defined even in the absence of kinematic cuts, we will in addition consider final-state cuts that will further help the separation of the Wt and $t\bar{t}$ processes. Such cuts, at variance with those of previous approaches (except ref. [9]), are easily applied in an experimental environment. The implementation of two definitions of the Wt channel in the same framework will allow us to estimate the theoretical systematics potentially affecting the extraction of the Wt signal from data. Although the implementation of any definition of the Wt channel into any higher-order computation is technically non-trivial (and MC@NLO is no exception to that), we argue and make it plausible that an NLO+parton shower framework is uniquely suited to the discussion of the physical consequences of such a definition.

The structure of the paper is as follows. In section 2 we give a first general discussion of the problem of interference with $t\bar{t}$ production. In section 3 we recall the various modes of single top quark production, before giving some technical details on the implementation of Wt production in MC@NLO, and on the underlying NLO computation. In section 4 we analyse the problem of interference in more detail, discuss the approaches in the literature, and propose two definitions of the Wt channel that can be used in a parton shower context and in an experimental analysis. We proceed in section 5 to present the results obtained by applying these two definitions in MC@NLO simulations. We discuss physical implications and conclude in section 6. Certain technical details are collected in the appendices.

2. Nature of the problem

In the perturbative computation of Wt production, one must consider all possible partonic processes with final states

$$t + W + \sum_i X_i \,. \tag{2.1}$$

Here, $\{X_i\}$ is a set of particles (partons in a QCD computation), whose multiplicity increases as the perturbative order increases. At the leading order (LO) in the SM, $\mathcal{O}(g_{\mathrm{w}}^2 \alpha_{\mathrm{s}})$, such a set is empty, and the underlying partonic process is

$$bg \longrightarrow tW \,. \tag{2.2}$$

When next-to-leading order (NLO) corrections in α_{s} are considered, contributions (e.g. $gg \to tW\bar{b}$) will appear such that

$$\{X_i\} \equiv \bar{b} \,. \tag{2.3}$$

Some of the relevant Feynman diagrams will feature the $W\bar{b}$ pair originating from a $\bar{t}$ internal line; in other words, the momentum flowing in the $\bar{t}$ propagator will

be $k_W + k_{\bar{b}}$. Therefore, in the computation of certain observables, one will need to integrate over the region

$$M_{\bar{b}W}^2 \equiv (k_W + k_{\bar{b}})^2 \simeq m_t^2 \,. \tag{2.4}$$

When this is the case, a divergence is encountered, which is regulated only by using a finite width for the (anti-)top, $\Gamma_t \neq 0$. However, a non-zero top width is an all-order result in g_{w}. Thus, the inclusion of higher-order QCD corrections forces one to include electroweak corrections to all orders so as to avoid divergences, and this potentially spoils the power counting in g_{w}, according to which eq. (2.2) is the LO contribution to tW production.

It turns out that indeed the region of eq. (2.4) causes severe problems, and as a result NLO QCD corrections are much larger than the LO result obtained with eq. (2.2). One possible way out is that of considering only observables which are exclusive enough to allow one to exclude, through final-state cuts, the resonance region eq. (2.4). This is easily done in a fixed-order, parton-level theoretical computation, where the W and the $\bar{b}$ are easily accessible. It becomes however a more indirect procedure in the context of a parton shower simulation, and impossible in a real experiment. Note also that, in order to avoid biases in an MC simulation, very loose cuts or no cuts at all will have to be imposed in the computation of underlying matrix elements, with the result that the majority of the events generated, being close to the $\bar{t}$ resonance, will actually be thrown away by final-state cuts, leading to a very low efficiency.

The dominance of the $\bar{t}$ resonance suggests that a possible approach is that of simply considering $W^+ W^- b\bar{b}$ final states (with the possibility of also including production spin correlations as well, for the fermions resulting from the decays of the W's – see e.g. ref. [14] for di-leptonic decays). In this way, what has previously been denoted as the LO contribution to Wt production, eq. (2.2), can be seen as a correction to $W^+ W^- b$ observables (i.e., observables inclusive in the final-state $\bar{b}$ present in the $W^+ W^- b\bar{b}$ matrix elements). The way in which this contribution is taken into account is a matter of careful definition, which is especially delicate (because of the double counting problem) when interfacing the matrix elements to parton showers – see what was done in ref. [9].

By emphasising the role of $W^+ W^- b(\bar{b})$ final states, these approaches have an immediate connection with data, and finding the Wt "signal" is thus a matter of a careful counting experiment. The key question is: are these predictions accurate enough for the counting to be reliable? Indeed, in these approaches the problem of full NLO corrections, whose knowledge is known to be crucial in top physics, is not considered.

The computation of NLO corrections to Wt production in QCD can only be seriously undertaken by recovering a meaningful definition of a perturbative expansion whose LO contribution is that of eq. (2.2). We have seen that the problem arises
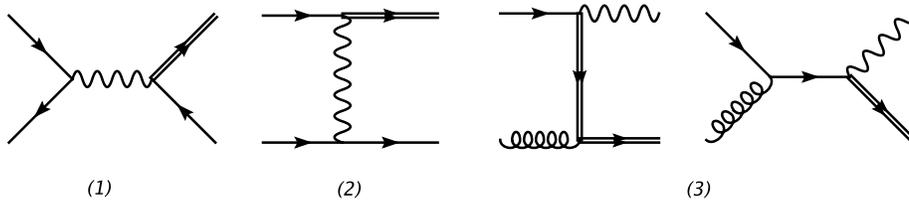
Figure 1: Leading order diagrams for single-t production in the (1) s-channel, (2) t-channel and (3) Wt-channel. The t-quark line is doubled.

because of the interplay between α_{s} and g_{w} expansions, and specifically because of the necessity of considering all-order contributions in g_{w}. The key observation is that the all-order result in g_{w} that we need is associated with a *decay*, whereas we are only interested in the role of EW interactions in the *production* process. A meaningful expansion in α_{s} of the Wt cross section could therefore be achieved if electroweak effects in production and decay could be disentangled. Such a procedure can never be fully consistent theoretically, but it can be given an operational meaning, which can be tested experimentally. The rest of the paper will be devoted to separating production and decay EW effects in the context of MC@NLO.

3. Wt production at NLO

In this section we introduce the various single top production modes at LO, before giving some details of the calculation of the Wt channel at NLO in QCD. Technical details regarding the implementation in MC@NLO are presented, although as these are similar to those relevant to the other single top production channels [5] we refer the reader to previous publications where appropriate. Since in this section we will be mainly concerned with the computation of the matrix elements entering the NLO predictions, and with the construction of the MC subtraction terms for MC@NLO, we can safely ignore the issues discussed in sect. 2, but will return to them in sect. 4.

3.1 Born level

There are three modes for the production of a single top quark at LO[1]. Each of these provides a separate and complementary means of studying the Wtb vertex: the s-channel mode (fig. 1(1)) involves a time-like, off-shell vector boson which may reveal new resonances; the t-channel mode (fig. 1(2)) involves a spacelike boson and is sensitive to flavour changing neutral currents (FCNC's). Finally, the Wt mode (fig.1(3)) has an on-shell W boson, and thus provides a complementary source of

---

[1]We assume throughout the paper that a 5 flavour scheme can be used for the quark sector, where the b quark is included in the initial state parton distributions. In principle the calculation could also be formulated in a 4 flavour scheme where all b quarks are generated in the final state.

information on the flavour structure of the vertex (i.e. V_{tb}), and its chiral properties. Based on expectations from the SM, this latter process has far too small a cross section to be observed at the Tevatron, but is expected to be significant at the LHC.

As shown in fig. 1(3), the lowest order partonic process for Wt production is

$$b(p_1) + g(p_2) \longrightarrow t(k_1) + W^-(k_2) \,. \tag{3.1}$$

Our description is confined to $W^-\bar{t}$ production. As explained in appendix A, for $W^+\bar{t}$ production no new diagrams need be computed, so that the description below suffices. Where no confusion is possible in the following, we denote the light quark attached to the Wt vertex as a b, implicitly representing any CKM-allowed down-type quark.

It is convenient to introduce the following invariants

$$s = (p_1+p_2)^2, \quad t_1 = t-m_t^2 = (k_1-p_1)^2-m_t^2, \quad u_1 = u-m_t^2 = (k_2-p_1)^2-m_t^2 \tag{3.2}$$

such that $s + t_1 + u_1 = m_W^2 - m_t^2$, with m_t denoting the top quark mass. We treat all other quarks as massless, including the b quark. The lowest order cross section can be written

$$d\sigma^{(0)} = \mathcal{M}^{(0)} d\phi_2 \,, \tag{3.3}$$

$$\mathcal{M}^{(0)} = \frac{1}{2s} \frac{1}{4} \frac{1}{N(N^2-1)} g_s^2 \frac{g_w^2}{8} |\mathcal{A}^{(0)}|^2 \tag{3.4}$$

where g_s, g_w are the QCD and EW coupling constants; N the number of colours; $d\phi_2$ denotes the two-body final state phase space, and the spin-summed Born-level matrix element is given by

$$\begin{aligned}
|\mathcal{A}^{(0)}|^2 = 16NC_F \Bigg\{ &-\left(\frac{s}{u_1} + \frac{u_1}{s}\right)\left(1 + \frac{m_t^2}{2m_W^2}\right) \\
&+ 2\frac{m_W^2(s+u_1)u_1 + m_t^2 m_W^2 s}{su_1^2}\left(1 - \frac{m_t^2}{2m_W^2} - \frac{m_t^4}{2m_W^4}\right) \\
&- \frac{m_W^4}{su_1}\left(2 - \frac{3m_t^2}{m_W^2} + \frac{m_t^6}{m_W^6}\right) - \frac{m_t^2}{m_W^2} \Bigg\} \,. \tag{3.5}
\end{aligned}$$

3.2 NLO computation

In order to implement a process in MC@NLO, one must cancel the singularities arising in the real and virtual graphs in the particular subtraction formalism of refs. [15, 16] and denoted FKS henceforth. In the FKS formalism, the NLO cross section is expressed in terms of the finite quantities that result from the cancellation of the (universal and process-independent) soft and collinear poles arising from virtual and real corrections. In order to obtain these finite quantities for a given process, one

needs the real matrix elements computed in 4 dimensions, and the virtual corrections computed in d dimensions. Although not strictly necessary in the FKS method, a d-dimensional virtual computation was carried out to fix the convention for its finite part.

The real and virtual matrix elements relevant to Wt production can be extracted from the NLO calculation of the Wc process [17], for which the diagrams are almost identical[2]. Given that the computation of ref. [17] adopted the phase-space slicing method [18, 19, 20] for cancelling the real and virtual singularities, we converted the conventions of the phase-space slicing into those of FKS. In order to check that this was carried out correctly, we repeated the calculation of the matrix elements.

3.2.1 Virtual corrections

As stated above, we calculated the one-loop virtual diagrams in dimensional regularisation in $d = 4 - 2\epsilon$ dimensions. Tensor and vector integrals were reduced to scalar integrals using the standard Passarino-Veltman algorithm [21]. For generation and evaluation of the relevant amplitudes, we utilised the Mathematica packages FeynArts [22] and FeynCalc [23], together with the FORM [24] computer program. As discussed previously, the results were checked against the virtual contributions obtained for Wc production in ref. [17], and found to be in agreement after the necessary analytical continuation (from $m_c < m_W$ to $m_t > m_W$). We have also checked, analytically and numerically, that our results for the scalar integrals are in agreement with those of ref. [25].

The virtual corrections are a Laurent series in the parameter ϵ, with double and single poles arising from soft, initial-state collinear, and ultraviolet (UV) singularities[3]. To remove UV poles we renormalise the top quark mass using an on-shell condition, with the QCD coupling in the $\overline{\text{MS}}$ scheme modified such that the top quark loop contribution is subtracted on-shell. This particular scheme [26] ensures that the top quark virtual contributions decouple in the limit of small external momenta. Specifically, the coupling is renormalised through next-to-leading order as

$$g_{\text{s}} \rightarrow g_{\text{s}}(\mu_{\text{R}}^2) \left[1 + \frac{\alpha_s(\mu_{\text{R}}^2)}{8\pi} \left(\frac{-1}{\epsilon} + \gamma_E - \ln 4\pi \right) \left(\frac{\mu_{\text{F}}^2}{\mu_{\text{R}}^2} \right)^\epsilon \beta_0 + \frac{\alpha_s(\mu_{\text{R}}^2)}{8\pi} \frac{2}{3} \ln \left(\frac{\mu_{\text{R}}^2}{m_t^2} \right) \right]$$
(3.6)

where μ_{F} is the factorisation scale, and μ_{R} the renormalisation scale. Furthermore, $\beta_0 = (11C_A - 2n_f)/3$ with n_f equal to the number of light flavors (here five) plus one. From this condition one can derive the following relation for the renormalised QCD coupling

$$\mu_{\text{R}}^2 \frac{dg_{\text{s}}(\mu_{\text{R}}^2)}{d\mu_{\text{R}}^2} = -g_{\text{s}}(\mu_{\text{R}}^2) \frac{\alpha_s(\mu_{\text{R}}^2)}{8\pi} \left(\beta_0 + \frac{2}{3} \right) + \mathcal{O}(g_{\text{s}}^5), \quad (3.7)$$

---

[2]Essentially, only the $W + (c\bar{c})$ channel has no analogue in the present case.

[3]Final-state collinear singularities are absent due to regularisation by the top mass.

which indeed removes the top quark loop from the β-function, such that the number of light flavours implemented in the code is n_f. The renormalisation of the top quark mass is given by

$$m_t \rightarrow m_t + \delta m_t =$$
$$m_t \left[1 + \frac{\alpha_{\rm S}(\mu_{\rm R}^2)}{4\pi} C_F \left(\frac{-3}{\epsilon} + 3\gamma_E - 3\ln 4\pi - 4 - 3\ln\left(\frac{\mu_{\rm R}^2}{m_t^2} \right) \right) \right] . \quad (3.8)$$

In contrast to the s and t single top production channels, the top quark occurs as an internal line in the Born amplitude. This gives rise to a contribution to the amplitude coming from the expansion of the renormalised top quark propagator

$$\frac{i}{\slashed{p} - (m_t + \delta m_t)} = \frac{i}{\slashed{p} - m_t} + \frac{i}{\slashed{p} - m_t}\delta m_t \frac{1}{\slashed{p} - m_t}. \quad (3.9)$$

The first term in this expansion gives the Born amplitude $\mathcal{A}^0$, whereas the second gives a modified amplitude $\mathcal{A}'^{(1)}$ involving the "squared" top quark propagator. In terms of the finite remainder of δm_t, the cross section receives the contribution

$$d\sigma_{\delta m_t}^{(1,V)} = (\delta m_t)_{\rm finite} \frac{1}{2s}\frac{1}{4}\frac{1}{N(N^2-1)} g_{\rm S}^2 \frac{g_{\rm W}^2}{8} \left(\mathcal{A}^{(0)}\mathcal{A}'^{\dagger(1)} + \mathcal{A}'^{(1)}\mathcal{A}^{\dagger(0)} \right) d\phi_2 , \quad (3.10)$$

where

$$\mathcal{A}^{(0)}\mathcal{A}'^{\dagger(1)} + \mathcal{A}'^{(1)}\mathcal{A}^{\dagger(0)} = -16NC_F \frac{m_t^2}{m_W^2 s u_1^3} \left\{ \left[4m_t^6 s + 4m_t^4 s(m_W^2 + u_1) \right] \right.$$
$$+ m_t^2 \left[-8m_W^4 s + 2m_W^2 s u_1 + u_1(u_1 + t_1)(s + 2t_1) \right]$$
$$\left. + u_1 \left[u_1 t_1(u_1 + t_1) + m_W^2(-s(u_1 - 2t_1) + 4t_1(u_1 + t_1)) \right] \right\} . \quad (3.11)$$

Following the renormalisation procedure, soft and collinear singularites remain and are proportional to the Born cross section such that the virtual terms may be written (c.f. eqs. (3.1) and (3.2) in ref. [15])

$$d\sigma^{(1,V)} = C_\epsilon g_{\rm S}^2 \left[-\frac{2}{\epsilon^2}(C_F + C_A) + \frac{2}{\epsilon}C_A \left(\ln\frac{s}{m_t^2} + \ln\frac{-u_1}{m_t^2} - \ln\frac{-t_1}{m_t^2} \right) \right.$$
$$\left. + \frac{1}{\epsilon}C_F \left(4\ln\frac{-t_1}{m_t^2} - 5 \right) - \frac{1}{\epsilon}\beta_0 \right] d\sigma_{4-2\epsilon}^{(0)} + d\sigma_{\rm finite}^{(1,V)}, \quad (3.12)$$

where $d\sigma_{4-2\epsilon}^{(0)}$ is the Born cross section in $4 - 2\epsilon$ dimensions, and

$$C_\epsilon = \frac{(4\pi e^{-\gamma_E})^\epsilon}{16\pi^2} \left(\frac{\mu_{\rm F}^2}{m_t^2} \right)^\epsilon . \quad (3.13)$$

These remaining poles are cancelled by similar singularities in the real contributions and by the collinear counterterms that arise from the renormalisation of the parton densities, in a form prescribed by the FKS formalism.

3.2.2 Real corrections

Since only initial-state collinear singularities are present in the process considered here, it is not necessary to partition the phase-space according to the FKS prescription, as done in ref. [5] for the case of s- and t-channel single-top production (see sect. 2.1.2 of that paper).

Therefore, the only technical difficulty in assembling the real corrections is in the explicit calculation of the diagrams[4]. As explain previously, we used the results of the Wc calculation presented in ref. [17]. There, the matrix elements were computed by considering the fictitious W boson decays

$$W(q) \longrightarrow Q(p) + \bar{b}_3(q_3) + g_4(q_4) + g_5(q_5) \tag{3.14}$$

and

$$W(q) \longrightarrow Q(p) + \bar{b}_3(q_3) + b_4(q_4) + \bar{b}_5(q_5), \tag{3.15}$$

where Q denotes generically the only quark with mass different from zero. These were decomposed into colour-ordered amplitudes, and computed using FORM [24]. The Wc and Wt matrix elements were subsequently obtained by crossing and summing over colour orders. This saved somewhat on computational effort, since the colour-ordered amplitudes served a second purpose, namely in the accounting of colour connections in the parton shower stage of the MC@NLO construction.

As a further check on the real computation, we compared the results we obtained from our calculation against the corresponding tree level matrix elements generated using the `MADGRAPH` program [27, 28]. We found agreement in all cases.

3.3 Implementation in MC@NLO

Several processes have by now been computed in the MC@NLO formalism, and we will therefore refrain from describing here the necessary steps for the implementation of a new reaction. The interested reader can find all details in refs. [3, 4, 5], which also report all the relevant analytic formulae we need (these are process-independent, and therefore no new computation is specifically required for Wt production). In this section, we will limit ourselves to giving the necessary information for the construction of the MC subtraction terms (which are process dependent) necessary for the matching of the NLO computation with HERWIG [29, 30].

One may write the MC subtraction terms as (see refs. [4, 5])

$$d\sigma\Big|_{\text{MC}} = \sum_i \sum_L \sum_l d\sigma_i^{(L,l)}\Big|_{\text{MC}}, \tag{3.16}$$

---

[4]There is a subtlety involving the construction of the local initial-state collinear counterterms used in numerical codes, as in all cases in which a gluon is exchanged. This issue is discussed in appendix B.

where i sums over the different partonic subprocesses, and $L \in \{+, -, f_1\}$ labels the parton leg from which the FKS parton is emitted (respectively: incoming parton along the $+z$ direction; incoming parton along the $-z$ direction; final state top quark). The index l runs over the different colour structures. If q_α and q_β denote the 4-momenta of the colour partners relevant to a given branching, the shower scale associated with the branching is

$$E_0^2 = |q_\alpha \cdot q_\beta|. \qquad (3.17)$$

The individual subtraction terms on the right-hand side of eq. (3.16) have the form (see eqs. (5.2)–(5.5) in ref. [4])

$$d\sigma_i^{(+,l)}\Big|_{\mathrm{MC}} = \frac{1}{z_+^{(l)}} f_a^{(H_1)}(\bar{x}_{1i}/z_+^{(l)}) f_b^{(H_2)}(\bar{x}_{2i}) \, d\hat{\sigma}_i^{(+,l)}\Big|_{\mathrm{MC}} d\bar{x}_{1i} \, d\bar{x}_{2i} \,, \qquad (3.18)$$

$$d\sigma_i^{(-,l)}\Big|_{\mathrm{MC}} = \frac{1}{z_-^{(l)}} f_a^{(H_1)}(\bar{x}_{1i}) f_b^{(H_2)}(\bar{x}_{2i}/z_-^{(l)}) \, d\hat{\sigma}_i^{(-,l)}\Big|_{\mathrm{MC}} d\bar{x}_{1i} \, d\bar{x}_{2i} \,, \qquad (3.19)$$

$$d\sigma_i^{(f_1,l)}\Big|_{\mathrm{MC}} = f_a^{(H_1)}(\bar{x}_{1f}) f_b^{(H_2)}(\bar{x}_{2f}) \, d\hat{\sigma}_i^{(f_1,l)}\Big|_{\mathrm{MC}} d\bar{x}_{1f} \, d\bar{x}_{2f} \,, \qquad (3.20)$$

where $f_{a,b}^{(H_{1,2})}$ are the initial state parton distributions, and z_L labels the partonic momentum fraction carried by the FKS parton. The short-distance cross sections $d\hat{\sigma}_i^{(L,l)}$ can be obtained from eqs. (5.6)–(5.8) of ref. [4]

$$d\hat{\sigma}_i^{(\pm,l)}\Big|_{\mathrm{MC}} = \frac{1}{\mathcal{N}} \frac{\alpha_{\mathrm{S}}}{2\pi} \frac{d\xi_\pm^{(l)}}{\xi_\pm^{(l)}} dz_\pm^{(l)} P_{a'b'}(z_\pm^{(l)}) \, d\bar{\sigma}_{i'} \Theta\left((z_\pm^{(l)})^2 - \xi_\pm^{(l)}\right); \qquad (3.21)$$

$$d\hat{\sigma}_i^{(f_1,l)}\Big|_{\mathrm{MC}} = \frac{\alpha_{\mathrm{S}}}{2\pi} \frac{d\xi_{f_1}^{(l)}}{\xi_{f_1}^{(l)}} dz_{f_1}^{(l)} P_{gq}(z_{f_1}^{(l)}) \, d\bar{\sigma}_{i'} \Theta\left(1 - \xi_{f_1}^{(l)}\right) \Theta\left(z_{f_1}^{(l)} - \frac{m_t}{E_0\sqrt{\xi_{f_1}^{(l)}}}\right), \qquad (3.22)$$

where $\mathcal{N} = 1$ for quark branchings, and 2 for gluon branchings (since the gluon has two colour partners); see refs. [4, 5] for the definition of $d\bar{\sigma}$. The various partonic subprocesses contributing to the Wt channel are listed in table 1 (the initial states bq and qb represent also $b\bar{q}$ and $\bar{q}b$). The shower scales to be used in eqs. (3.21) and (3.22) are equal to the absolute values of the dot products given in table 1. From table 1, we see that $\mathcal{N} = 2$ for all branchings in the processes with $\{b, q\}$, $\{b, \bar{b}\}$ and $\{b, b\}$ initial states, and for branchings from leg $-$ and leg $+$ in the processes $(b, g; t, W, g)$ and $(g, b; t, W, g)$ respectively.

When interfacing the NLO calculation with a parton shower, it is also necessary to supply a colour flow to the Monte Carlo. When a given subprocess can have more than one colour flow, the one that is given to the parton shower is chosen on a statistical basis. The weights that govern these probabilities are formed using leading order (in the number of colours N) approximations to the squared matrix elements of the corresponding tree-level diagrams. In our case, these have already been calculated,

NLO	$(b,g;t,W)$	$(g,b;t,W)$
$(g,g;t,W,\bar{b})$	$+(\bar{p}_1\cdot\bar{p}_2)$	$-(\bar{p}_1\cdot\bar{p}_2)$
$(b,q;t,W,q)$	$-(\bar{p}_1\cdot\bar{p}_2,\bar{p}_2\cdot\bar{k}_1)$	
$(q,b;t,W,q)$		$+(\bar{p}_1\cdot\bar{p}_2,\bar{p}_1\cdot\bar{k}_1)$
$(b,\bar{b};t,W,\bar{b})$	$-(\bar{p}_1\cdot\bar{p}_2,\bar{p}_2\cdot\bar{k}_1)$	
$(\bar{b},b;t,W,\bar{b})$		$+(\bar{p}_1\cdot\bar{p}_2,\bar{p}_1\cdot\bar{k}_1)$
$(b,b;t,W,b)$	$-(\bar{p}_1\cdot\bar{p}_2,\bar{p}_2\cdot\bar{k}_1)$	$+(\bar{p}_1\cdot\bar{p}_2,\bar{p}_1\cdot\bar{k}_1)$
$(b,g;t,W,g)$	$+,f_1(\bar{p}_1\cdot\bar{k}_1);\ -(\bar{p}_1\cdot\bar{p}_2,\bar{p}_2\cdot\bar{k}_1)$	
$(g,b;t,W,g)$		$-,f_1(\bar{p}_2\cdot\bar{k}_1);\ +(\bar{p}_1\cdot\bar{p}_2,\bar{p}_1\cdot\bar{k}_1)$

Table 1: Short-distance contributions to MC subtraction terms. The two columns correspond to the two possible Born cross sections. For a given process, the entries show the emitting legs, and in round brackets the value(s) of the shower scale(s) E_0^2 (up to a sign).

as the real emission contributions were computed using colour ordered amplitudes. Given that there is a one-to-one mapping between the colour ordered amplitudes and the various colour flows, one can choose to use these colour ordered amplitudes in the statistical determination of the colour flow[5].

4. Interference between $t\bar{t}$ and Wt production

In section 3 we have discussed the calculation of the Wt cross section within the FKS subtraction formalism, and its subsequent implementation in MC@NLO. However, the use of such a Monte Carlo event generator assumes that the Wt channel is well-defined beyond LO. In fact, as already outlined in sect. 2, this is not the case, and the theoretical definition of this production channel is not straightforward.

At LO, the Wt pair is produced through the reaction of eq. (3.1), and its cross section is smaller than that of top pair production by a factor of about 15. Beyond LO, some of the Feynman graphs that contribute to the Wt channel and that are dominant in the region of eq. (2.4) are shown in fig. 2. These diagrams can be interpreted as the production of a $t\bar{t}$ pair at LO, with subsequent decay of the $\bar{t}$ into a $\bar{b}W$ pair. It follows that the set of Feynman graphs contributing to $gg \to tW\bar{b}$ or $q\bar{q} \to tW\bar{b}$ can be divided into two subsets, that are customarily denoted as *doubly resonant* and *singly resonant*, the former being those depicted in fig. 2 or analogous ones. The problem discussed in sect. 2 can be formulated in terms of the interference between these two subsets of graphs, and physically interpreted as the interference between Wt and $t\bar{t}$ production. This interpretation is consistent with our aim of

---

[5]Other choices are possible, as one is free to modify the above procedure by terms subleading in the number of colours N.
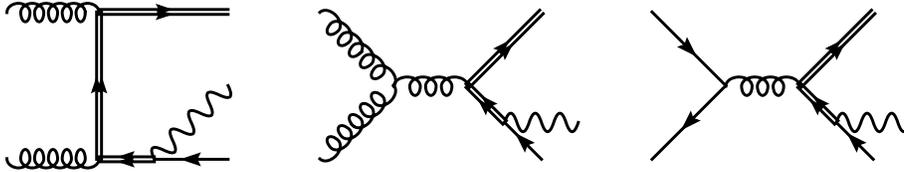
Figure 2: Diagrams that are doubly-resonant, in the sense that the intermediate $\bar{t}$ can be on-shell.

emphasising the role of electroweak interactions in the production mechanism of the t and of the W. The interference would not cause any problem if the contribution from the doubly-resonant diagrams was small. However, a large increase of the cross section occurs when the $\bar{t}$ propagator becomes resonant i.e. in the kinematic region of eq. (2.4). It follows that the naïve calculation of the Wt channel, defined as that resulting from the straightforward computation of Feynman diagram as discussed in sect. 3, becomes meaningless in perturbation theory. In this section, we will discuss how it is possible to separate out Wt and $t\bar{t}$ production, and recover a workable definition of the Wt channel.

4.1 Previous approaches

This interference problem has already been discussed in several papers. Given that the problem here only arises for gg and $q\bar{q}$ initial states, present in real-emission processes, it is not peculiar to full higher-order computations, but also occurs in those that only include tree-level graphs. Each of the previous Wt computations beyond LO has introduced a strategy for isolating the Wt production channel. We briefly discuss each of them in turn.

In ref. [8], the suggestion was made to place a cut on the invariant mass $M_{\bar{b}W}$ of the $W\bar{b}$ pair, which can be written in the form:

$$|M_{\bar{b}W} - m_t| > \kappa\Gamma_t, \tag{4.1}$$

where Γ_t is the width of the top quark. This cut thus removes events from the region of phase space corresponding to the $\bar{t}$ resonance. It efficiently reduces the $t\bar{t}$ interference to the Wt channel, but cannot be directly applied in an event generation/experimental situation, where one is unable to unambiguously identify the b quark and W boson which originate in the hard interaction.

In ref. [7], the Wt signal is defined by subtracting, at the level of squared amplitudes, the $t\bar{t}$ cross section multiplied by $t \to Wb$ branching ratio; the procedure is defined in a fully-inclusive way. A comparison was made with the invariant mass cut approach of ref. [8], and the resulting cross section found to agree if the choice $\kappa \sim 15$ was made.

As discussed in sect. 2, the approach of ref. [9] addresses the problem in a more general context, i.e. that of simulating $W^+W^-b(\bar{b})$ production in a realistic parton-shower environment. As such, the definition of the Wt channel does not need to be directly considered, except for the necessity of avoiding double counting. This way of by-passing the interference problem is correct, and facilitates the comparison with data. However, it does not allow one to include the full NLO corrections into the results, because of both problems of practice (the relevant one-loop, six-point amplitudes – or eight-point amplitudes, if fully decayed W's are considered – are not available yet), and of principle (how to combine the one-loop contribution for W^+W^-b with the rest).

The full NLO computation of ref. [10] follows the same type of strategy as ref. [7], where the total cross section is modified by a subtraction term which effectively removes the $t\bar{t}$-like contribution. However, few details on how this subtraction term is defined are given. The results are presented only for total rates.

Finally, a definition of the Wt channel within a fully differential NLO computation was presented in ref. [11]. There, the suggestion was made to place a cut on the transverse momentum p_{T}^b of the "additional b quark that appears at the next-to-leading order" [11], namely the b quark that appears in the diagrams of fig. 2, which accompanies the b quark coming from the decay of the top (not shown in fig. 2). In practice, this amounts to keeping events that satisfy

$$p_{\mathrm{T}}^b < p_{\mathrm{T}}^{(veto)}, \tag{4.2}$$

where appropriate. This means that in the case of partonic processes with no such additional b quark, no veto is applied. The reasoning for the condition in eq. (4.2) is that harder b quarks tend to have come from the decay of a top, and thus the probability for producing events with two hard b quarks is dominated by the contribution of diagrams with a t and a $\bar{t}$ both on-shell or almost on-shell. By requiring the additional b to be softer, one thus reduces the interference between the doubly resonant diagrams and the singly resonant diagrams which are identified with the Wt channel. Furthermore in ref. [11], the factorisation scale is chosen to be equal to $p_{\mathrm{T}}^{(veto)}$. If this condition is not met, doubly-resonant diagrams are removed from the computation at the amplitude level. Finally, processes with a $q\bar{q}$ initial state are not included, independently of the choice of factorisation scale. This is only a problem of principle, since in practice the numerical impact of such processes is so small that they can be neglected. As in the other calculations discussed above, it is not possible to apply this definition of the Wt channel in an event generation/experimental situation, since the veto is based on a partonic picture at a given order in α_{s}.

4.2 MC@NLO approach

In this section, we consider the problem of defining the Wt channel in a way that is applicable in an event generator context, where both initial- and final-state parton

showers are present. Although none of the approaches discussed in subsection 4.1 can be directly applied in this situation, they can be used to some degree in motivating suitable solutions.

The simplest and most drastic solution is to remove from the computation the contributions of those processes which contain doubly-resonant diagrams. At the NLO, this amounts to removing *completely* diagrams having gg or $q\bar{q}$ initial states, i.e. regardless of whether or not they are doubly resonant. As far as the $q\bar{q}$ contribution is concerned, this is what is done in MCFM [11]. It is not quite the same as what is done for the gg initial state, but is numerically very close to that, owing to the combination of the veto, and of the choice of the factorisation scale $\mu_{\mathrm{F}} = p_{\mathrm{T}}^{(veto)}$. However, even if one generalises the definition of the veto to apply in a parton shower context (as we will do in the following), the removal of processes characterised by a particular initial state is theoretically unfeasible. Firstly, renormalisation group invariance is violated such that the underlying NLO calculation has the same formal scale dependence as a LO one (thus undermining one of the motivations for using an NLO generator at all). Secondly, and perhaps more seriously, partonic processes mix as soon as higher-order effects are considered, as happens when initial-state showers are present. Thus, we discount this method as a viable means of separating out the Wt channel in a full Monte Carlo generator and do not present further results from it here.

Instead, we present two definitions of the Wt channel, that are designed in such a way that, by comparing them, one can directly assess the impact of the interference with $t\bar{t}$. Thus, if the results from the two definitions agree, we can be confident of having isolated the Wt channel. Such an agreement, when it occurs, is the result both of the definitions themselves, and of final-state cuts which may or may not be applied. It is important to stress that the definitions that we shall give are meaningful even without any subsequent cuts. This engenders a greater degree of flexibility in the practical investigation of whether the Wt channel is well defined or not.

Our two definitions can be summarised as follows:

1. Diagram Removal (DR). Here one simply removes all diagrams in the NLO Wt amplitudes that are doubly resonant (i.e. those diagrams shown in figure 2).

2. Diagram Subtraction (DS). In this approach, one modifies the NLO Wt cross section by implementing a subtraction term designed to cancel *locally* the $t\bar{t}$ contribution.

Note that DR is different from the removal of gg- and $q\bar{q}$-initiated processes discussed previously, since diagrams with these initial states are kept if they are not doubly resonant. Note also that the DS procedure is similar to what has been proposed in ref. [7], but the construction of its local subtraction term involves some technical complications, which we discuss later.

In order to discuss in detail the DR and DS definitions, we introduce some notation. Let us denote by $\mathcal{A}_{\alpha\beta}$ the $\mathcal{O}(g_{\mathrm{w}}\alpha_{\mathrm{s}})$ amplitude of the process:

$$\alpha(p_1) + \beta(p_2) \longrightarrow t(k_1) + W(k_2) + \delta(k) \,. \tag{4.3}$$

The precise identity of parton δ is not relevant for what follows, so we omit it from the notation. We have:

$$\mathcal{A}_{\alpha\beta} = \mathcal{A}_{\alpha\beta}^{(Wt)} + \mathcal{A}_{\alpha\beta}^{(t\bar{t})} \,, \tag{4.4}$$

where the two terms on the r.h.s. are the respective contributions of the singly- and doubly-resonant diagrams to the naïve Wt cross section. In the computation of the cross section at NLO, the following quantity appears:

$$|\mathcal{A}_{\alpha\beta}|^2 = \left|\mathcal{A}_{\alpha\beta}^{(Wt)}\right|^2 + 2\Re\left\{\mathcal{A}_{\alpha\beta}^{(Wt)}\mathcal{A}_{\alpha\beta}^{(t\bar{t})\star}\right\} + \left|\mathcal{A}_{\alpha\beta}^{(t\bar{t})}\right|^2 \tag{4.5}$$

$$\equiv \mathcal{S}_{\alpha\beta} + \mathcal{I}_{\alpha\beta} + \mathcal{D}_{\alpha\beta} \,. \tag{4.6}$$

We stress that the terms $\mathcal{I}_{\alpha\beta}$ and $\mathcal{D}_{\alpha\beta}$ are non-zero only in the cases of $\{\alpha, \beta\} = \{g, g\}$ and $\{q, \bar{q}\}$, where in the latter process q may also be a b quark. In these cases, δ will be a $\bar{b}$ quark or another down-type antiquark according to the CKM matrix. Furthermore, $\mathcal{D}_{\alpha\beta}$ has neither soft nor collinear singularities, while those of $\mathcal{I}_{\alpha\beta}$ are integrable and subleading w.r.t. those of $\mathcal{S}_{\alpha\beta}$. Therefore, in the context of an NLO computation in the FKS formalism (or for that matter in any subtraction formalism), the NLO real-emission contribution to the subtracted short-distance partonic cross section including the flux factor and phase space will be:

$$d\hat{\sigma}_{\alpha\beta} = \frac{1}{2s}\left(\hat{\mathcal{S}}_{\alpha\beta} + \mathcal{I}_{\alpha\beta} + \mathcal{D}_{\alpha\beta}\right)d\phi_3 \,, \tag{4.7}$$

where the hat denotes that infrared singularities have been suitably subtracted. It is understood that the subtraction is performed by means of plus-type distributions, which therefore may apply to the phase space as well. The hadroproduction cross section resulting from eq. (4.7) is

$$d\sigma = d\sigma^{(2)} + \sum_{\alpha\beta} \int dx_1 dx_2 \mathcal{L}_{\alpha\beta} d\hat{\sigma}_{\alpha\beta}$$

$$= d\sigma^{(2)} + \sum_{\alpha\beta} \int \frac{dx_1 dx_2}{2x_1 x_2 S} \mathcal{L}_{\alpha\beta}\left(\hat{\mathcal{S}}_{\alpha\beta} + \mathcal{I}_{\alpha\beta} + \mathcal{D}_{\alpha\beta}\right)d\phi_3 \,, \tag{4.8}$$

with S the squared centre of mass energy of the colliding hadrons and $\mathcal{L}_{\alpha\beta}$ the parton-level luminosity. The quantity $d\sigma^{(2)}$, requiring a two-body phase space, denotes all contributions to the cross sections that are not already included in eq. (4.7), i.e. the Born, soft-virtual, and collinear remainder terms. Both $d\sigma^{(2)}$ and eq. (4.7) (but not their sum, eq. (4.8)) are convention-dependent, since finite pieces can be freely moved from one contribution to the other, but this is irrelevant for the following discussion.

When the NLO computation is then matched to parton showers according to the MC@NLO prescription, the above equation must be modified by the subtraction of MC counterterms. We can choose to absorb these in $\hat{\mathcal{S}}_{\alpha\beta}$, because this is the only piece that contains leading soft and collinear singularities. Thus the schematic form of eq. (4.8) applies at both the NLO and MC@NLO levels. In this notation, the DR cross section corresponds to:

$$d\sigma^{(\text{DR})} = d\sigma^{(2)} + \sum_{\alpha\beta} \int \frac{dx_1 dx_2}{2x_1 x_2 S} \mathcal{L}_{\alpha\beta} \hat{\mathcal{S}}_{\alpha\beta} d\phi_3 \,, \tag{4.9}$$

i.e. there are now no terms $\mathcal{I}_{\alpha\beta}$ or $\mathcal{D}_{\alpha\beta}$, as all doubly resonant diagrams have been removed from the *amplitude*. As mentioned previously, this cross section violates gauge invariance; this issue will be discussed in sect. 5.2.

Starting from eq. (4.8), we also define the DS cross section. This amounts to writing:

$$d\sigma^{(\text{DS})} = d\sigma - d\sigma^{subt} \,, \tag{4.10}$$

where $d\sigma^{subt}$ is designed to remove numerically the doubly-resonant contribution. This may be achieved locally by defining

$$d\sigma^{subt} = \sum_{\alpha\beta} \int dx_1 dx_2 \, \mathcal{L}_{\alpha\beta} \, d\sigma_{\alpha\beta}^{subt} \,; \tag{4.11}$$

$$d\sigma_{\alpha\beta}^{subt} = \frac{1}{2s} \widetilde{\mathcal{D}}_{\alpha\beta} d\phi_3 \,, \tag{4.12}$$

such that the quantity

$$\mathcal{D}_{\alpha\beta} - \widetilde{\mathcal{D}}_{\alpha\beta} \tag{4.13}$$

will vanish when $M_{\bar{b}W}^2 \equiv (k + k_2)^2 \to m_t^2$. Note that $\mathcal{D}_{\alpha\beta}$ and $\widetilde{\mathcal{D}}_{\alpha\beta}$ themselves will, in such a limit, either diverge, if $\Gamma_t = 0$, or have a Breit-Wigner-like peak, if $\Gamma_t \neq 0$. The DS cross section in eq. (4.10) can now be re-written in the same form as eq. (4.9):

$$d\sigma^{(\text{DS})} = d\sigma^{(2)} + \sum_{\alpha\beta} \int \frac{dx_1 dx_2}{2x_1 x_2 S} \mathcal{L}_{\alpha\beta} \left(\hat{\mathcal{S}}_{\alpha\beta} + \mathcal{I}_{\alpha\beta} + \mathcal{D}_{\alpha\beta} - \widetilde{\mathcal{D}}_{\alpha\beta} \right) d\phi_3 \,. \tag{4.14}$$

One sees that the difference between the DR and DS cross sections has the form:

$$d\sigma^{(\text{DS})} - d\sigma^{(\text{DR})} = \sum_{\alpha\beta} \int \frac{dx_1 dx_2}{2x_1 x_2 S} \mathcal{L}_{\alpha\beta} \left(\mathcal{I}_{\alpha\beta} + \mathcal{D}_{\alpha\beta} - \widetilde{\mathcal{D}}_{\alpha\beta} \right) d\phi_3 \,, \tag{4.15}$$

and thus is composed of a contribution from the interference term, and of the difference between the subtraction term and the true doubly resonant contribution to the NLO cross section.

Our aim is now to construct a gauge-invariant subtraction term, such that the difference $\mathcal{D}_{\alpha\beta} - \widetilde{\mathcal{D}}_{\alpha\beta}$ is as close to zero as possible. Note also that requiring the

subtraction term to be local and gauge invariant prevents this difference from being identically zero. The subtraction term should have the schematic form:

$$\widetilde{\mathcal{D}}_{\alpha\beta} = |\mathcal{A}^{(0)}(\alpha\beta \to t\bar{t})|^2 \times \text{BW}(M_{\bar{b}W}) \times |\mathcal{A}^{(0)}(\bar{t} \to W\bar{b})|^2 \qquad (4.16)$$

where $\mathcal{A}^{(0)}(\alpha\beta \to t\bar{t})$ is the LO (i.e., $\mathcal{O}(\alpha_{\mathrm{s}})$) top pair production amplitude, $\mathcal{A}^{(0)}(\bar{t} \to W\bar{b})$ the decay amplitude of the anti-top, and $\text{BW}(M_{\bar{b}W})$ is the Breit-Wigner function.

The first obvious difficulty in constructing a workable implementation of eq. (4.16) is that the kinematics on the l.h.s. should be that of the full $\alpha\beta \to tW\bar{b}$ process (due to the requirement of local cancellation in eq. (4.14)), whereas at the same time the $\bar{t}$ needs to be on-shell in order to compute the quantity $\mathcal{A}^{(0)}(\alpha\beta \to t\bar{t})$ in a gauge-invariant way. A second difficulty is that, while $\mathcal{A}^{(0)}(\alpha\beta \to t\bar{t})$ is computed with top width $\Gamma_t = 0$, the Breit-Wigner factor in eq. (4.16) requires non-zero Γ_t.

As a first attempt to overcome these difficulties one can reshuffle the momenta of the decay products, to obtain an on-shell $\bar{t}$ quark. In this case, one uses a non-zero top width only in the Breit-Wigner factor. However, a more fundamental problem with eq. (4.16) is that spin correlations are not included, thus spoiling again the local cancellation property we seek to achieve. Therefore, rather than eq. (4.16), we need a subtraction term of the form:

$$\widetilde{\mathcal{D}}_{\alpha\beta} = \left| \mathcal{A}^{(t\bar{t})}_{\alpha\beta} \right|^2_{\text{reshuffled}}, \qquad (4.17)$$

where $\mathcal{A}^{(t\bar{t})}_{\alpha\beta}$ is defined in eq. (4.4). In other words, $\widetilde{\mathcal{D}}_{\alpha\beta}$ would be identical to $\mathcal{D}_{\alpha\beta}$, were it not for the reshuffling. Being a full amplitude, eq. (4.17) does implement spin correlations in the decay of the $\bar{t}$. A divergence present in eq. (4.17) when $\Gamma_t = 0$ disappears by setting $\Gamma_t \neq 0$. However, the reshuffling implies that $\widetilde{\mathcal{D}}_{\alpha\beta}$ is not likely to have the Breit-Wigner shape in $M_{\bar{b}W}$ that would be desirable in order for the difference in eq. (4.13) to be as small as possible in the whole phase space. This is easily rectified by defining:

$$\widetilde{\mathcal{D}}_{\alpha\beta} = \frac{BW(M_{\bar{b}W})}{BW(m_t)} \left| \mathcal{A}^{(t\bar{t})}_{\alpha\beta} \right|^2_{\text{reshuffled}}. \qquad (4.18)$$

By construction, the amplitude of this subtraction term at $M_{\bar{b}W} = m_t$ is precisely such as to cancel the resonant contribution to the NLO Wt cross-section.

However, even after this modification, there is a problem. For appropriate cancellations of collinear singularities, we would also have to use $\Gamma_t \neq 0$ in the computation of $|\mathcal{A}_{\alpha\beta}|^2$. Unfortunately, after setting $\Gamma_t \neq 0$ in the radiative amplitudes in this way, their collinear limits are modified, and in order not to disrupt the local cancellation of collinear divergences one would need to perform the full calculation adopting a framework for the consistent inclusion of finite-width effects in all kinematic regions

of interest (e.g. the complex mass scheme [31]). Given the scope of the present paper, a more pragmatic approach suffices, which has been extensively used at LEP in dealing with resonant decays. Namely, we set $\Gamma_t \neq 0$ only in the doubly-resonant diagrams, and leave $\Gamma_t = 0$ in the singly-resonant ones. This strategy is straightforward to implement in `MADGRAPH`.

5. Results

In the previous section we discussed the problem of interference between $t\bar{t}$-like amplitudes (followed by decay of the $\bar{t}$) and Wt-like amplitudes. Two separation mechanisms, DR and DS, were defined as being suitable for an all orders computation of the scattering amplitude, as occurs in a Monte Carlo event generator. We have implemented both of these separation mechanisms in the MC@NLO framework, as discussed in sect. 3. We stress that the MC subtraction terms given in sect. 3 are identical for DS and DR, since such terms only modify (w.r.t. a pure-NLO computation) the form of $\hat{\mathcal{S}}_{\alpha\beta}$, which is identical in the DS and DR cross sections. In this section we present sample results, and compare in detail the output of the DS and DR calculations. Our aim is to analyse, from a perturbative point of view, the degree to which separation of the Wt channel is possible, thus giving an upper bound for the impact of the interference that can be obtained with a realistic analysis. Detailed phenomenological results will not be presented here, but are postponed to a forthcoming publication. In particular, we only consider fully leptonic decays of the final-state W bosons, as these are sufficient to furnish a comparison between the different separation mechanisms. In practice, semileptonic rather than fully leptonic decays will be studied first by experiments at the LHC. Furthermore, our results are obtained by neglecting production spin correlations, which is not restrictive as far as comparing the two definitions of the Wt channel given here is concerned. We have however implemented spin correlations in the DR calculation, using the method of ref. [6]. Their implementation in the DS calculation along those lines is technically slightly more complicated (but possible), owing to the negativity of the "squared" matrix elements at some phase-space points (due to the subtraction term), and is also deferred to the future.

All of the following numerical results have been obtained for the LHC with the MRST2002 default PDF set [32], setting the top mass and width to $m_t = 170.9$ GeV and $\Gamma_t = 1.41$ GeV, as well as the W mass and width to $m_W = 80.4$ GeV and $\Gamma_W = 2.141$ GeV. The default values of the renormalisation and factorisation scales are equal to the top mass. The LO results quoted in this section have been obtained using the same parameters (including PDFs and two-loop α_s) as those adopted for NLO computations.

5.1 Transverse momentum veto

As discussed previously, the definitions we gave of the Wt channel are independent of any cuts that are subsequently used to further reduce the interference from $t\bar{t}$ production. Nevertheless, it is unrealistic to define the Wt channel, in an actual experimental environment, with no cuts[6] at all. It is not the purpose of this paper to undertake a thorough investigation of various cut strategies. Therefore, we shall limit our considerations to one particular cut, motivated by the transverse momentum veto proposed in ref. [11], and discussed here in sect. 4.1. As stated there, the veto acts on the additional b quark that may be present at the NLO level. Here we generalise this idea to an event generator context i.e. to a situation in which we cannot tell with certainty which parton or hadron is associated with the additional b quark.

Firstly, one searches all b-flavoured hadrons in a given event, and orders them in transverse momentum (or transverse energy). All hadrons whose pseudorapidity η_B is outside a given range, which we choose to be

$$|\eta_B| \leq 2.5\,, \tag{5.1}$$

are ignored. Secondly, a veto analogous to that of eq. (4.2) is applied on the transverse momentum (or transverse energy) of the second hardest B hadron satisfying eq. (5.1):

$$p_{\mathrm{T}}^B < p_{\mathrm{T}}^{(veto)}. \tag{5.2}$$

In cases where no second-hardest B hadron satisfying the above requirements can be found, the event is accepted. Note that this is the case in processes which do interfere with $t\bar{t}$ production, but in which a b quark is replaced by another down-type quark – an effect off-diagonal in the CKM matrix. In this paper, we assume a 100% b-tagging efficiency. However, it is clear that the veto procedure proposed here can be applied in more realistic b-tagging scenarios. A more detailed phenomenological investigation of this issue is postponed to a future publication.

In a realistic analysis the veto would be accompanied by a number of further cuts. For example, in the semileptonic decay mode, the veto can be used in combination with a jet topology cut, to further reduce the contamination of the Wt "signal" from $t\bar{t}$ "background". Given that such cuts are absent in the results presented here, our findings correspond to a somewhat pessimistic scenario as far as the purity of the Wt signal is concerned.

The definition of the veto adopted here can also be used in the context of a pure-NLO, parton-level computation, such as that of ref. [11], by simply replacing B hadrons with b quarks[7]. It is instructive to see, however, that the veto is a much more

---

[6]We mean here cuts whose *only purpose* is that of separating the Wt and $t\bar{t}$ processes, and not generic selection cuts aimed at selecting the t and/or the W in a collision event.

[7]b quarks can also be considered in an MC context. We have found that MC@NLO results obtained by imposing b quark vetos are very similar to those obtained with B hadron vetos.

natural constraint in an event generator context than in a parton-level, fixed-order computation. In table 2 we present the results for the DR and DS total cross sections,

MC@NLO					NLO				
$\sigma^{(\mathrm{DR})}$	$\sigma^{(\mathrm{DS})}$	$\sigma^{(\mathrm{LO})}$	$K^{(\mathrm{DR})}$	$K^{(\mathrm{DS})}$	$\sigma^{(\mathrm{DR})}$	$\sigma^{(\mathrm{DS})}$	$\sigma^{(\mathrm{LO})}$	$K^{(\mathrm{DR})}$	$K^{(\mathrm{DS})}$
$p_{\mathrm{T}}^{(veto)} = 10$ GeV									
34.66	33.89	26.60	1.30	1.27	35.05	34.74	34.67	1.01	1.00
$p_{\mathrm{T}}^{(veto)} = 30$ GeV									
41.86	40.74	31.85	1.31	1.28	39.93	39.67	34.67	1.15	1.14
$p_{\mathrm{T}}^{(veto)} = 50$ GeV									
44.61	42.92	33.71	1.32	1.27	42.81	42.00	34.67	1.23	1.21
$p_{\mathrm{T}}^{(veto)} = 70$ GeV									
45.63	43.65	34.31	1.33	1.27	44.41	42.90	34.67	1.28	1.24
$p_{\mathrm{T}}^{(veto)} = \infty$									
46.33	44.12	34.67	1.34	1.27	46.33	44.12	34.67	1.34	1.27

Table 2: Results for the total DR, DS, and leading order cross sections (in pb), obtained with MC@NLO (five left columns) and our pure-NLO parton level computation (five right columns). See the text for details. The notation $p_{\mathrm{T}}^{(veto)} = \infty$ denotes no veto at all.

obtained with MC@NLO and with our pure-NLO parton level computation. We also give the results (denoted by $\sigma^{(\mathrm{LO})}$) obtained in the two frameworks by keeping only LO matrix elements. In the case of MC@NLO, $\sigma^{(\mathrm{LO})}$ is thus equal to what one would get by simply running HERWIG standalone[8]. The table finally reports the values of the ratios of NLO over LO cross sections:

$$K^{(\mathrm{DR})} = \frac{\sigma^{(\mathrm{DR})}}{\sigma^{(\mathrm{LO})}}, \qquad K^{(\mathrm{DS})} = \frac{\sigma^{(\mathrm{DS})}}{\sigma^{(\mathrm{LO})}}. \qquad (5.3)$$

In the fixed-order computation at LO, there is simply no second-hardest b quark, and $\sigma^{(\mathrm{LO})}$ is therefore independent of the value of $p_{\mathrm{T}}^{(veto)}$. On the other hand, in an MC context the initial-state b quark entering the hard partonic process at LO eventually results, because of parton showers, in the generation of a B hadron. Therefore, $\sigma^{(\mathrm{LO})}$ computed with an event generator does depend on $p_{\mathrm{T}}^{(veto)}$. The interesting thing about this dependence is that it appears to be the same as that obtained at the NLO, as can be inferred from the basically constant values of $K^{(\mathrm{DR})}$ and $K^{(\mathrm{DS})}$ obtained with MC@NLO. This is not the case for the parton-level fixed-order computation, where

---

[8]In fact, Wt production is not implemented in HERWIG. We simply computed the LO matrix elements, and used the Les Houches interface [33] to give HERWIG the hard events, as in the case of MC@NLO.

the factors K display a significant dependence upon $p_{\mathrm{T}}^{(veto)}$. This raises the following two issues. At small-p_{T}, the fixed-order results lack Sudakov suppression at $p_{\mathrm{T}}^b \to 0$; it follows that the predictions obtained for small values of $p_{\mathrm{T}}^{(veto)}$ are not particularly meaningful. At larger p_{T}'s, the real-emission matrix elements dominate, and an NLO computation is expected to be reliable. Unfortunately, since the veto does not enter the LO results, it is not possible to sensibly estimate the impact of higher-order corrections: small changes to $p_{\mathrm{T}}^{(veto)}$ lead to large changes in the factors K, which may effectively mask the impact of $t\bar{t}$ interference. In summary, the imposition of a veto appears to be somewhat problematic in parton-level, fixed-order computations. This issue would imply a much (perhaps overly) larger theoretical systematic error, relative to an MC-based simulation, in the comparison between predictions and data.

5.2 Gauge (in)dependence of DR cross sections

As pointed out in sect. 4.2, the definition of the DR cross section, in which certain diagrams are removed from an amplitude, is not gauge invariant. In this section, we will argue that this is not a problem in practice, by repeating the DR calculation in a number of alternative gauges. We have checked several different observables, namely the total cross section; single-inclusive rapidity and transverse momentum distributions of the t, W and their decay products; and azimuthal and transverse momentum correlations between the charged leptons. We present here results for the total cross section and the transverse momentum $p_{\mathrm{T}}^{(ll)}$ of the charged lepton pair. These are representative of the corresponding results for other observables.

Our original calculation of the NLO cross section in the DR approach was carried out in the Feynman gauge, where the gluon propagator is given by:

$$D_{\mu\nu} = -\frac{g_{\mu\nu}}{k^2} \,. \tag{5.4}$$

The sum over the polarisation degrees of freedom of initial-state gluons has been restricted to transverse polarisations. In order to check the sensitivity to the choice of gauge, we repeated the calculation in various covariant and non-covariant gauges. We summarise these results as follows.

First, we note that the gauge dependence can only enter in the gg channel. This is because only diagrams involving two external gluons have broken gauge invariance, and these occur in the qg and gg channels. However, the qg channel has no resonant diagrams, thus no diagrams are removed. The diagrams kept in the gg channel (before crossing) are shown in figure 3. Only the third diagram in figure 3 leads to a gauge dependence, due to the presence of the gluon propagator. One can consider the general family of covariant gauges that result from replacing the propagator of eq. (5.4) with:

$$D_{\mu\nu} = -\frac{1}{k^2} \left(g_{\mu\nu} + (1-\lambda)\frac{k_\mu k_\nu}{k^2} \right) \,. \tag{5.5}$$
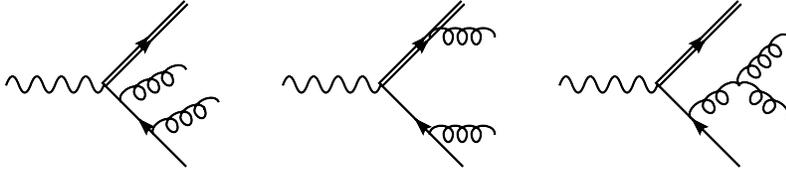
Figure 3: Diagrams kept in the gg channel after removing resonant contributions, shown before crossing. These formally represent also the two additional diagrams in which the two gluons arising from the fermion line have their momenta exchanged.

This is useful, as $\lambda = 1$ reproduces the Feynman gauge calculation. One thus has a continuous parameter in the DR calculation, such that it tends smoothly to the Feynman gauge calculation in a well-defined limit. However, it is easily seen from the form of the three gluon vertex that the second term in eq. (5.5) decouples from the amplitude. Thus, DR results do not depend on the choice of gauge within the family of covariant gauges.

One may also consider non-covariant gauges, in which the gluon propagator is given by[9]:

$$D_{\mu\nu} = \left[-g_{\mu\nu} + \frac{n_\mu k_\nu + n_\nu k_\mu}{n \cdot k} - \frac{n^2 k_\mu k_\nu}{(n \cdot k)^2} \right] \frac{1}{k^2}. \tag{5.6}$$

The third term decouples for the same reason as in a covariant gauge, but a gauge dependence results from the second term. Here we report the numerical results for the MC@NLO cross section in DR, obtained with non-covariant gauges, for the three choices $n^2 > 0$, $n^2 = 0$, and $n^2 < 0$. We start in table 3 with the results obtained by integrating over the whole phase space, except perhaps for the veto imposed on the second-hardest B hadron of the event (see sect. 5.1). For reference, we also report the results obtained in the Feynman gauge (which is our default). We define a relative difference as follows:

$$\delta = 10^3 \times \frac{\sigma^{\text{(DR)}}(\text{non} - \text{covariant}) - \sigma^{\text{(DR)}}(\text{covariant})}{\sigma^{\text{(DR)}}(\text{covariant})}. \tag{5.7}$$

We observe very small relative differences, which are actually compatible with zero within the statistical errors of our runs (each of which consists of 500k events). Note that this conclusion holds regardless of whether a veto is imposed or not.

We have also checked that the same conclusion applies to more exclusive observables. It is obviously impossible to reach the same level of statistical accuracy as that in table 3 for a differential distribution, especially in the tails of the transverse

---

[9]The gluon propagator also depends in general on a gauge-fixing parameter α, which we set equal to zero in what follows. See e.g. refs. [34, 35].

$p_{\rm T}^{(veto)} = 10$		$p_{\rm T}^{(veto)} = 30$		$p_{\rm T}^{(veto)} = 50$		$p_{\rm T}^{(veto)} = 70$		$p_{\rm T}^{(veto)} = \infty$	
σ	δ	σ	δ	σ	δ	σ	δ	σ	δ
Covariant									
34.66	0	41.86	0	44.61	0	45.63	0	46.33	0
$n^2 > 0$									
34.70	1.15	41.90	0.96	44.70	2.01	45.73	2.19	46.42	1.94
$n^2 = 0$									
34.75	2.60	41.94	1.91	44.69	1.79	45.71	1.75	46.42	1.94
$n^2 < 0$									
34.70	1.15	41.87	0.24	44.61	0	45.63	0	46.37	0.86

Table 3: Gauge dependence of DR rates. The cross sections σ are given in pb, and veto values $p_{\rm T}^{(veto)}$ in GeV. Note the factor 10^3 in the definition of δ, eq. (5.7). The notation $p_{\rm T}^{(veto)} = \infty$ denotes no veto at all.

momentum spectra which fall rather steeply. We have computed the ratios

$$R(\mathcal{O}) = \frac{d\sigma^{(\rm DR)}}{d\mathcal{O}}(\text{non}-\text{covariant}) \Big/ \frac{d\sigma^{(\rm DR)}}{d\mathcal{O}}(\text{covariant}) \qquad (5.8)$$

bin-by-bin for the observables $\mathcal{O}$ (we have considered rapidities and transverse momenta, both for single-inclusive observables and for correlations), and found all ratios to be compatible with one. The typical value of $|R(\mathcal{O}) - 1|$ is actually always much smaller than the statistical error affecting this quantity. The latter may be of the order of a few tens of percent in individual bins in the tails of $p_{\rm T}$ distributions. However, since bin-by-bin fluctuations tend to integrate to zero if several contiguous bins are considered, we also fitted ratios in eq. (5.8) for those cases in which $\mathcal{O}$ is a transverse momentum, by assigning arbitrarily the same 0.1% relative errors to all bins, with the functional form

$$a_1 + a_2 p_{\rm T} + a_3 p_{\rm T}^2 \,. \qquad (5.9)$$

This ensures that the tail of the $p_{\rm T}$ distributions is treated in the fit on the same footing as the peak region, thus dealing in an efficient way with the problem of bin-by-bin fluctuations, and allowing us to uncover hints of non-flatness in $R(p_{\rm T})$ as a function of $p_{\rm T}$. In this way, we have again found that all $R(p_{\rm T})$ we have considered are compatible with one in the whole $p_{\rm T}$ range. As an example, we present here the results obtained for the transverse momentum $p_{\rm T}^{(ll)}$ of the lepton pair, for the four veto choices, and for the gauge $n^2 > 0$. The ratio $R(p_{\rm T}^{(ll)})$ are presented in the upper pane of fig. 4. The result is also given for the case in which no veto at all is applied. As
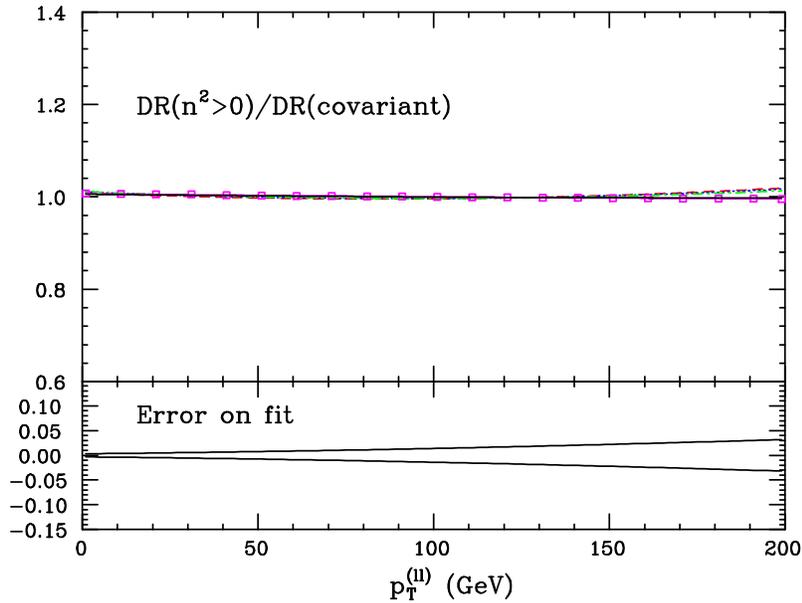
Figure 4: Gauge dependence of the DR cross section, as a function of the p_{T} of the lepton pair, for a non-covariant gauge with $n^2 > 0$. Upper pane: results of the fits, using the form in eq. (5.9). Lower pane: envelope of curves obtained by varying all parameters of the fit within their error ranges (see the text for details), divided by the best fit curve, minus one. Black solid, red dashed, blue dotted, and green dot-dashed lines correspond to $p_{\mathrm{T}}^{(veto)} = 10$, 30, 50, and 70 GeV respectively. The magenta solid line with open boxes is obtained without imposing any veto.

one can see from the figure, all curves resulting from the fit are remarkably flat (they cannot actually be easily distinguished). Some of them may be seen to depart from one at the largest $p_{\mathrm{T}}^{(ll)}$ values, but this behaviour is not statistically significant. To show this, we present in the lower pane of fig. 4 the envelope of the curves obtained by considering all combinations of values $a_i = a_i^0 \pm \Delta(a_i)$, with a_i^0 and $\Delta(a_i)$ being the best values and their fitting errors respectively (as given by MINUIT [36]). The envelope is then divided by the best fit curve and unity is subtracted, so as to give an upper bound for the error affecting the fitting procedure. Only the result relevant to $p_{\mathrm{T}}^{(veto)} = 10$ GeV is presented in the lower pane of fig. 4, since all the others are essentially identical.

We therefore conclude that, regardless of the observable studied, the impact of gauge dependence in the DR computation can be safely neglected in the numerical studies that follow.

5.3 Impact of interference

In order to gauge how much of the difference between DS and DR is due to the

interference term alone, it is useful to define the quantity:

$$d\sigma^{(\text{NI})} = d\sigma^{(2)} + \sum_I \int \frac{dx_1 dx_2}{2x_1 x_2 S} \mathcal{L}_{\alpha\beta} \left(\hat{\mathcal{S}}_{\alpha\beta} + \mathcal{D}_{\alpha\beta} - \widetilde{\mathcal{D}}_{\alpha\beta} \right) d\phi_3 \,, \qquad (5.10)$$

where the label NI stands for *non-interference*. Clearly

$$d\sigma^{(\text{DS})} - d\sigma^{(\text{NI})} = \sum_I \int \frac{dx_1 dx_2}{2x_1 x_2 S} \mathcal{L}_{\alpha\beta} \mathcal{I}_{\alpha\beta} d\phi_3 \,, \qquad (5.11)$$

which is then a direct estimate of the interference contribution, free of contaminations due to doubly-resonant contributions which are present in eq. (4.15). Although eq. (5.11) is not a physical quantity, it is useful to compute it because of the expression for $d\sigma^{(\text{DS})} - d\sigma^{(\text{DR})}$ in eq. (4.15). As can be seen there, this quantity is the interference term eq. (5.11), plus the difference between the doubly-resonant contribution and the subtraction term. Thus, eq. (5.11) would be identical to $d\sigma^{(\text{DS})} - d\sigma^{(\text{DR})}$ in the limiting case $\mathcal{D} \equiv \widetilde{\mathcal{D}}$ (which, we recall, is impossible to achieve if local cancellation and gauge invariance are simultaneously imposed).

Results for the total cross sections after implementation in MC@NLO are shown in table 4, where we have defined the relative differences:

$$\delta_1 = \frac{\sigma^{(\text{DS})} - \sigma^{(\text{DR})}}{\sigma^{(\text{DR})}} \,, \qquad (5.12)$$

$$\delta_2 = \frac{\sigma^{(\text{DS})} - \sigma^{(\text{NI})}}{\sigma^{(\text{DR})}} \,. \qquad (5.13)$$

Overall, we observe that the relative differences are not large, and decrease for tighter vetoes. This is to be expected given that by requiring a stricter veto, one filters out more of the $t\bar{t}$ process. Note that the relative differences due to the interference term alone are larger than those between DR and DS, implying that the terms $\mathcal{I}$ and $\mathcal{D} - \widetilde{\mathcal{D}}$ cancel out to some extent.

Although not reported in this table, we have studied the scale dependence of these results, by varying the renormalisation and factorisation scales between $m_t/2$ and $2m_t$. The two scales are always set equal to a common value, which is somewhat restrictive but sufficient for our present purposes. Although the individual cross sections depend very mildly on scales (the variations w.r.t. the central values being $^{+2}_{-3}\%$, $^{+1}_{-2}\%$, and $^{+3}_{-4}\%$ for DR, DS, and NI respectively), this is not the case for $\sigma^{(\text{DS})} - \sigma^{(\text{DR})}$ and $\sigma^{(\text{DS})} - \sigma^{(\text{NI})}$, which have variations w.r.t. their central values of about $\pm 20\%$ and $\pm 30\%$ respectively. This behaviour is not surprising: the individual cross sections have been defined with the specific purpose of describing the Wt cross section, which is known from the literature to have a mild scale dependence. On the other hand, as explicitly shown in eqs. (4.15) and (5.11), the differences of cross sections considered in table 4 are dominated by LO $t\bar{t}$ production, which has a significant scale dependence (see e.g. ref. [37] for a recent update).

$\sigma^{(\mathrm{DR})}$	$\sigma^{(\mathrm{DS})}$	$\sigma^{(\mathrm{NI})}$	$\sigma^{(\mathrm{DS})} - \sigma^{(\mathrm{DR})}$	δ_1	$\sigma^{(\mathrm{DS})} - \sigma^{(\mathrm{NI})}$	δ_2
$p_{\mathrm{T}}^{(veto)} = 10$ GeV						
34.66	33.89	35.08	-0.77	-2.2%	-1.19	-3.4%
$p_{\mathrm{T}}^{(veto)} = 30$ GeV						
41.86	40.74	42.83	-1.12	-2.7%	-2.09	-5.0%
$p_{\mathrm{T}}^{(veto)} = 50$ GeV						
44.61	42.92	46.59	-1.69	-3.8%	-3.67	-8.2%
$p_{\mathrm{T}}^{(veto)} = 70$ GeV						
45.63	43.65	48.24	-1.98	-4.3%	-4.59	-10.0%
$p_{\mathrm{T}}^{(veto)} = \infty$						
46.33	44.12	49.58	-2.21	-4.8%	-5.46	-11.8%

Table 4: Results for the total DR, DS, and NI cross sections (in pb) defined in eqs. (4.9), (4.14), and (5.10), for various values of the veto. We also give the relative differences as defined in eqs. (5.12) and (5.13). The notation $p_{\mathrm{T}}^{(veto)} = \infty$ denotes no veto at all.

We have also carried out similar studies on differential distributions. The results presented in table 4 are, not surprisingly, dominated by the small transverse momentum regions, where the bulk of the cross section lies. Analogously to what was done in eq. (5.8), we have computed the ratios

$$R^{(\mathrm{DS})}(\mathcal{O}) = \frac{d\sigma^{(\mathrm{DS})}}{d\mathcal{O}} \bigg/ \frac{d\sigma^{(\mathrm{DR})}}{d\mathcal{O}}\,, \qquad R^{(\mathrm{NI})}(\mathcal{O}) = \frac{d\sigma^{(\mathrm{NI})}}{d\mathcal{O}} \bigg/ \frac{d\sigma^{(\mathrm{DR})}}{d\mathcal{O}}\,, \qquad (5.14)$$

for several observables. In the cases in which $\mathcal{O}$ is a rapidity, these ratios are flat over the whole kinematically-accessible range, with values consistent with those given in table 4. The situation is more interesting if one considers transverse momenta, since in such cases the ratios in eq. (5.14) display a non-trivial shape. In particular, the largest values of $\left|R^{(\mathrm{DS})} - 1\right|$ and $\left|R^{(\mathrm{NI})} - 1\right|$, amongst the observables we have studied, are found in the tail of $p_{\mathrm{T}}^{(ll)}$ (which is the reason why this observable has been considered as a case study in this paper).

We start by presenting results for the quantities defined in eq. (5.14). In order to be able to superimpose five curves on the same plot and keep visibility (since histograms would blur the picture because of bin-by-bin fluctuations in the tail), the ratios have again been fitted with the functional form of eq. (5.9). The results are given in the upper panes of fig. 5. As can be seen from the figure, the impact of interference can be very large for large enough values of $p_{\mathrm{T}}^{(ll)}$, regardless of the choice for $p_{\mathrm{T}}^{(veto)}$ (although, of course, it is less significant for small vetos). It must be stressed however that, at large $p_{\mathrm{T}}^{(ll)}$, the cross section is small. This is documented
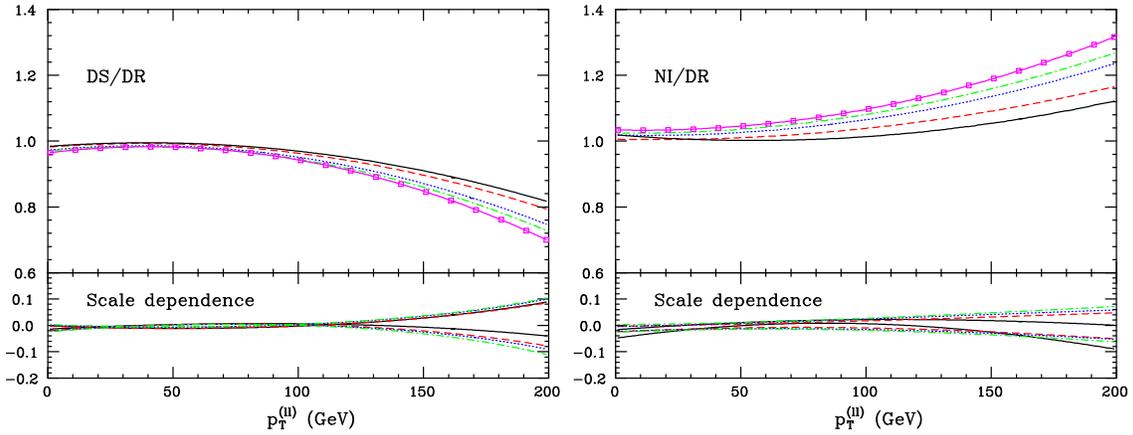
Figure 5: Upper panes: results for the ratios defined in eq. (5.14), as a function of $p_{\mathrm{T}}^{(ll)}$ and for various vetos. Lower panes: relative scale dependence (see eq. (5.16)). The linestyles are the same as those of fig. 4.
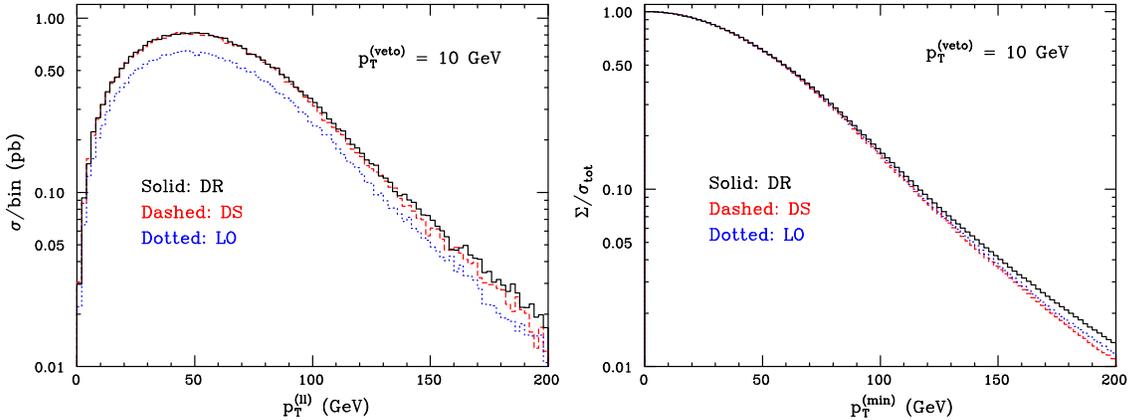
Figure 6: Left pane: differential DR, DS, and LO distributions in $p_{\mathrm{T}}^{(ll)}$. Right pane: integral of the same distributions in the range $p_{\mathrm{T}}^{(min)} < p_{\mathrm{T}}^{(ll)} < \infty$, divided by the respective total rates. These results are relevant to the case $p_{\mathrm{T}}^{(veto)} = 10$ GeV.

in fig. 6, where we present in the left pane the differential distributions in $p_{\mathrm{T}}^{(ll)}$, as computed with DR, DS, and at LO. The same information is presented in the right pane of the figure, in an integral form:

$$\frac{1}{\sigma_{tot}}\Sigma(p_{\mathrm{T}}^{(min)}) = \frac{1}{\sigma_{tot}}\int_{p_{\mathrm{T}}^{(min)}}^{\infty} dp_{\mathrm{T}}^{(ll)} \frac{d\sigma}{dp_{\mathrm{T}}^{(ll)}} . \tag{5.15}$$

The results of fig. 6 have been obtained by choosing $p_{\mathrm{T}}^{(veto)} = 10$ GeV. Although the absolute value of the differential cross section has a non-negligible dependence on $p_{\mathrm{T}}^{(veto)}$, its shape is relatively stable against variations of $p_{\mathrm{T}}^{(veto)}$. Thus, the right pane of fig. 6 can be used with table 4 for estimating the number of events with

$p_\mathrm{T}^{(ll)} \geq p_\mathrm{T}^{(min)}$ for any choice of the veto (or in its absence).

The comparison between fig. 5 and fig. 6 shows that, for the majority of events, the impact of interference is moderate. On the other hand, these results imply that conclusions concerning interference of Wt with $t\bar{t}$ are observable dependent. One particular analysis may be sensitive to an observable which receives much larger contributions from $\mathcal{I}$ and $\mathcal{D} - \widetilde{\mathcal{D}}$ than the total rate. With fig. 5 we have presented a worst-case scenario among the observables studied.

It is also interesting to study the scale dependence of these results. This cannot be done in the same way as for the total rates of table 4. There, differences of cross sections have been considered, and the relative variation w.r.t. the central values computed. In the case of the tail of a steeply falling differential distribution, bin-by-bin differences lead to such small numbers that it is impossible, in practice, to obtain a statistically significant result for the relative variation, since the latter would be a ratio of two extremely small numbers. On the other hand, we are able to compute the scale dependence of the ratios defined in eq. (5.14). In the lower panes of fig. 5, we present the quantities

$$\frac{R^{(\mathrm{DS})}\left(p_\mathrm{T}^{(ll)}; \mu_\mathrm{F} = \mu_\mathrm{R} = \kappa m_t\right)}{R^{(\mathrm{DS})}\left(p_\mathrm{T}^{(ll)}; \mu_\mathrm{F} = \mu_\mathrm{R} = m_t\right)} - 1, \qquad \kappa = 1/2, 2 \tag{5.16}$$

(and the analogous one for NI) as a function of $p_\mathrm{T}^{(ll)}$. Equation (5.16) will not give directly the scale dependence of a $t\bar{t}$-dominated cross section, as was the case for the differences of rates of table 4, but rather that of the fraction of the DS and NI cross sections arising from $t\bar{t}$-like contributions. As can be seen from the figure, the scale dependence of such a fraction is largest in the region where the interference between singly- and doubly-resonant diagrams is largest. This is consistent with the naïve expectation that Wt-like contributions have a much milder scale dependence than $t\bar{t}$-like ones. On the other hand, the study of scale dependence shows that the qualitative conclusion that one draws from fig. 5 is perturbatively stable, and that the interference is significant only in the large-p_T region.

6. Discussion

In this paper we have presented the first calculation of single-top production in association with a W boson, accurate to NLO in QCD and interfaced with parton showers according to the MC@NLO formalism. In studying the Wt channel, our main aim has been to investigate whether or not one can define it as a separate production process, since only in the case of a positive answer is the computation of the full NLO corrections meaningful and feasible with present technologies. The NLO+parton shower framework provides an excellent platform for addressing the

problem. Parton showers give the capability of studying final states in a realistic environment, and testing ideas that can be applied without any modifications to an experimental analysis. The underlying NLO computation is, on the other hand, directly sensitive to interference effects with $t\bar{t}$ production.

We have considered two separation mechanisms for defining the Wt channel: diagram removal (DR) and diagram subtraction (DS). We have defined them in such a way that it is not necessary, in order to generate full hadronic events with high efficiency, to apply any kinematic cuts. In this way complete flexibility is achieved, to study the effects of any cuts whose aim is that of enhancing the Wt "signal" w.r.t the $t\bar{t}$ "background". As an example, we have considered only one such cut, namely a veto on the transverse momentum of the second-hardest B hadron of the event.

The DR cross section is obtained by removing the doubly-resonant diagrams from the calculation of the Wt *amplitude*, and thus violates gauge invariance. We have demonstrated that this is not a problem in practice. The DS cross section involves a modification of the naïve Wt *cross-section* by a gauge invariant subtraction term which acts to remove the doubly-resonant contribution from $t\bar{t}$ final states. Given that this is done at the cross-section level, an interference term between the $t\bar{t}$ and Wt processes remains.

Ultimately, we are in a position to decide whether it is possible, and useful for data analysis, to define the Wt channel as a production process in its own right. The key question is whether an approximate treatment of interference within a higher-order computation has to be preferred, for the sake of a counting experiment, to an exact treatment of interference without QCD corrections. Furthermore, the separation of Wt and $t\bar{t}$ processes allows one to consider NLO Wt results (which are $\mathcal{O}(g_{\mathrm{w}}^2\alpha_{\mathrm{s}}^2)$) alongside NLO $t\bar{t}$ results (which are $\mathcal{O}(\alpha_{\mathrm{s}}^3)$). This makes a realistic description of phenomenology possible (since it is well known that higher-order corrections for $t\bar{t}$ production are crucial in this respect), in spite of being unable to treat the problem exactly in its full complexity. In this paper we have found that NLO corrections are larger than interference effects, especially if cuts are employed that are designed to enhance the Wt signature. The answer to the above question therefore appears to be *yes*. However, the definitions that render it possible to compute higher-order corrections also imply an ambiguity in the theoretical predictions, that we identify with the difference between DR and DS cross sections. We have found that such an ambiguity is observable-dependent, and in particular is larger in those regions of the phase space that correspond to large transverse momenta. Since this ambiguity will be directly related to the theoretical systematic error, it follows that the accuracy with which Wt properties can be measured depends on the observables that are most relevant to a given analysis.

To conclude, having implemented the Wt production mode in an NLO plus parton shower context, we find based on our subsequent analysis that it does indeed seem feasible to analyse this process at the LHC.

Acknowledgments

A. W^-t and $W^+\bar{t}$ production

In this appendix we demonstrate that the squared amplitudes for single top production with an associated W boson are independent of whether the final state top is a quark or an antiquark.

Firstly there is the issue of a possible charge asymmetry due to the electroweak coupling of the W boson. This merely constrains the helicity of the fermion line which includes the top quark in the graph, which occurs either as an open line or a closed loop. The $t \to \bar{t}$ transformation changes the direction of the line, and leads to a constraint on the helicity of the corresponding antifermion line. However, the sign and size of the coupling is the same in both cases.

Furthermore, there is the issue of a possible QCD asymmetry. One must consider in more detail the open or closed fermion loop associated with the top quark (and the b quark from top decay). The replacement $t \to \bar{t}$ can affect the amplitude in two ways:

1. It changes the sign of all momenta which occur in uncut propagators along the top quark line[10]. If p_i are the propagating momenta, the fermion trace in each diagram will contain the following terms:

$$(\not{p}_1 - m_t)(\not{p}_2 - m_t)\dots(\not{p}_M - m_t), \qquad (A.1)$$

where M is the number of uncut fermion momenta, and there may be additional Dirac matrices between the propagator factors. Interchanging top and antitop quarks gives instead the terms

$$(-\not{p}_1 - m_t)(-\not{p}_2 - m_t)\dots(-\not{p}_M - m_t) = (-1)^M(\not{p}_1 + m_t)(\not{p}_2 + m_t)\dots(\not{p}_M + m_t). \qquad (A.2)$$

---

[10]Cut propagators correspond to terms in the fermion trace of form $\not{p} \pm m_t$ depending on whether quark or antiquark spinors are involved i.e. the sign of the momentum is not changed.

Given that the number of Dirac matrices in each interference graph is even, only terms involving an even number of masses survive. Then the amplitude for antiquark production is related to that for quark production via

$$\mathcal{A}_{\bar{t}} = C_{diag}\mathcal{A}_t$$
$$= (-1)^M \mathcal{A}_t, \tag{A.3}$$

where $\mathcal{A}_{t,\bar{t}}$ is the amplitude associated with a given interference diagram. Here C_{diag} is the parity under $t \to \bar{t}$ of the diagram i.e. $C_{diag} = \pm 1$.

2. The colour factor may be affected. In each of the diagrams for Wt production, one always has

$$\mathcal{C}_{\bar{t}} = C_{col}\mathcal{C}_t, \tag{A.4}$$

where $\mathcal{C}_{t,\bar{t}}$ are the colour factors for the amplitude with a top and antitop quark respectively, and $C_{col} = \pm 1$.

The total parity under $t \to \bar{t}$ is then given by

$$C = C_{diag}C_{col} = \pm 1. \tag{A.5}$$

Squared real emission diagrams will always have an even number of uncut propagators, and also symmetric colour factors under $t \to \bar{t}$. Regarding interference diagrams, there are 48 in total. These can be subdivided into gg, bb, bg and $b\bar{b}$ initial states. Then diagrams with other quarks in the initial state form a subset of those already specified. The gg and $b\bar{b}$ diagrams are always associated with real emissions. For the bb (and, hence, qq) initial state, there is only one Feynman amplitude and hence no interference term is possible. The qg initial states can be associated with real or virtual emissions. By evaluating the number of uncut fermion propagators and the colour factor for each graph, one can find its parity under $t \to \bar{t}$ using eq. (A.5).

There are two types of diagrams:

1. Diagrams with no triple gluon coupling. These all have symmetric colour factors under $t \to \bar{t}$, and an even number of uncut fermion propagators. Hence $C = 1$ for such graphs.

2. Diagrams with a triple gluon coupling. These all have antisymmetric colour factors, and an odd number of uncut fermion propagators (this latter fact can be easily appreciated by considering removing a gluon line from a fermion in graphs of type 1 and reattaching it to a gluon line). Hence $C = (-1)^2 = +1$ for these graphs.

One finds that every graph is even upon replacing top quarks by antitop quarks, and so the total squared amplitude for Wt production is the same for both t and $\bar{t}$.

Even if W^-t and $W^+\bar{t}$ matrix elements are identical at this order, there is still the possibility of a charge asymmetry arising from differences between the b and $\bar{b}$ parton densities[11]. However, these densities are equal in the global fits available at present. Thus, overall, the cross-sections and differential distributions considered here for top and anti-top production are strictly equal.

B. Calculation of $\tilde{\mathcal{M}}$ in the helicity formalism

NLO subtraction formalisms such as FKS achieve a good numerical stability through the local cancellation between large contributions of opposite sign, which correspond to the real-emission matrix elements in the soft and collinear regions, and the counterterms. The counterterms are in fact constructed by calculating the above limits of the matrix elements, whose form is universal. If one considers e.g. the initial-state collinear limit $p_2 \parallel k$ of the process

$$\alpha(p_1) + \beta(p_2) \longrightarrow X(K) + \delta(k) \,, \tag{B.1}$$

with X a set of final state particles which are not relevant here (in our case, $X \equiv t + W$), the matrix element squared is (see e.g. eq. (B.41) of ref. [15])

$$\mathcal{M}(p_1, p_2) \xrightarrow{p_2 \parallel k} \frac{4\pi\alpha_{\mathrm{S}}}{k \cdot p_2} \left[P(z)\mathcal{M}^{(0)}(p_1, zp_2) + Q(z)\tilde{\mathcal{M}}(p_1, zp_2) \right] \,, \tag{B.2}$$

where P are the usual Altarelli-Parisi kernels, Q are other universal kernels (given at the leading order in eqs. (B.42)–(B.45) of ref. [15] for initial-state collinear splittings, and in eqs. (B.31)–(B.34) of that paper for final-state collinear splittings; these kernels are thus different for spacelike and timelike branchings already at the leading order), $\mathcal{M}^{(0)}$ is the relevant Born contribution, and $\tilde{\mathcal{M}}$ is a Born-like function, which however keeps track of the azimuthal correlations in the branching process. The contribution of $Q\tilde{\mathcal{M}}$ vanishes upon integration over the azimuthal angle of the branching, which is why this term can be neglected in the analytical computation of the collinear divergences in $4 - 2\epsilon$ dimensions. Locally, it is different from zero if the parton involved in the branching which enters the hard reaction is a gluon, and therefore needs to be taken into account for the construction of the local counterterms in a (efficient) numerical NLO program.

Unlike the case of s- and t-channel single-top production, the Wt channel has a gluon entering the hard reaction at the Born level, and we thus need to compute the relevant $\tilde{\mathcal{M}}$ (which is process dependent, whereas the kernels Q are universal). This

---

[11]As already discussed in refs. [7, 11].
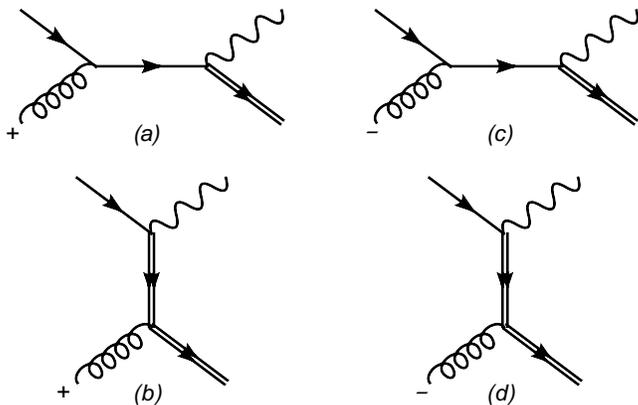
Figure 7: Diagrams used in the calculation of $\tilde{\mathcal{M}}$ for $0 \to b(p_1) + g(p_2) + W^-(p_3) + t(p_4)$, i.e. all momenta are defined to be outgoing.

term is (see eq. (B.23) of ref. [15])

$$\tilde{\mathcal{M}} = \mathcal{F} \operatorname{Re} \left\{ \frac{\langle kp_2 \rangle}{[kp_2]} \mathcal{A}_+^{(0)\dagger} \mathcal{A}_-^{(0)} \right\}, \tag{B.3}$$

with $\mathcal{A}_\pm^{(0)}$ the Born amplitude for Wt production with a positive/negative helicity initial state gluon respectively, and $\mathcal{F}$ a term which includes the flux and spin- and colour-average factors, and the coupling constants. We have computed the r.h.s. of eq. (B.3) in two independent ways, and found agreement. In this appendix we present some details on how the computation can be carried out by using spinor helicity methods [38, 39, 40, 41, 42]. As is conventional when applying such methods, we take all momenta to be *outgoing* in this appendix, in contrast to the rest of the paper. Furthermore, we relabel the outgoing momenta k_2, k_1 as p_3 and p_4 respectively (see fig. 7), in order to be able to use a compact notation in what follows.

The relevant diagrams are illustrated in fig. 7. Besides the null momenta p_1 and p_2, we define the null vector

$$p_5 = p_4 - \frac{m_t^2}{u_1} p_2, \tag{B.4}$$

where $u_1 = u - m_t^2 = (p_2 + p_4)^2 - m_t^2$. As is common, we adopt the notation

$$|k^\pm\rangle \equiv u_\pm(k), \quad \langle k^\pm| \equiv \bar{u}_\pm(k) \tag{B.5}$$

for massless quark spinors. Defining the Mandelstam invariants

$$s = (p_1 + p_2)^2; \quad t = (p_1 + p_4)^2, \tag{B.6}$$

33

the contributions $\mathcal{A}_+^{(s)}$ and $\mathcal{A}_+^{(u)}$ of the positive helicity diagrams (denoted by (a) and (b) respectively in fig. 7) are given by (neglecting colour factors)

$$\mathcal{A}_+^{(s)} = -\frac{2i\sqrt{2}}{s\langle 12\rangle}\epsilon_\mu(p_3)\bar{u}(p_4)\gamma^\mu|2-\rangle\langle 21\rangle\langle 2+|u(p_1); \tag{B.7}$$

$$\mathcal{A}_+^{(u)} = \frac{2i\sqrt{2}}{u_1\langle 12\rangle}\epsilon_\mu(p_3)\bar{u}(p_4)\left[|1+\rangle[25]\langle 5-| + m|2-\rangle\langle 1-|\right]\gamma^\mu u(p_1), \tag{B.8}$$

where $\epsilon_\mu(p_3)$ is the polarisation vector of the W boson, and we have used the standard notation

$$[ij] = \langle i+|j-\rangle, \quad \langle ij\rangle = \langle i-|j+\rangle. \tag{B.9}$$

In deriving eqs. (B.7) and (B.8) we have used the following expressions for the gluon polarisation vectors

$$\epsilon_{+,\mu}(p_2, q) = \frac{\langle q-|\gamma_\mu|2-\rangle}{\sqrt{2}\langle q2\rangle}, \quad \epsilon_{-,\mu}(p_2, q) = \frac{\langle q+|\gamma_\mu|2+\rangle}{\sqrt{2}[2q]}. \tag{B.10}$$

Here q is an arbitrary null reference momentum, which has been set to p_1. One is in principle able to choose a different reference momentum for the negative helicity diagrams, owing to the fact that helicity amplitudes are separately gauge invariant. However, if one also chooses $q_2 = p_1$ in the negative helicity case then diagram (c) in fig. 7 vanishes. This relies on the helicity of the light quark line being fixed by the chiral boson coupling. Then the negative helicity amplitude is given solely by diagram (d):

$$\mathcal{A}_-^{(0)} = \frac{2i\sqrt{2}}{u_1[21]}\epsilon_\mu(p_3)\bar{u}(p_4)\left[\frac{u}{u_1}|2+\rangle[12]\langle 2-| + |2+\rangle[15]\langle 5-| + m_t|1-\rangle\langle 2-|\right]\gamma^\mu u(p_1). \tag{B.11}$$

It can be checked that $|\mathcal{A}_+^{(0)}|^2 + |\mathcal{A}_-^{(0)}|^2$, after summing over the W boson and quark spins, is equal to the known Born result, eq. (3.5). For the helicity interference term, one uses eqs. (B.7), (B.8), and (B.11) to find $(\mathcal{A}_+^{(0)} = \mathcal{A}_+^{(s)} + \mathcal{A}_+^{(u)})$:

$$\mathcal{A}_+^{(0)\dagger}\mathcal{A}_-^{(0)} = \frac{8}{u_1^2 m_W^2}\frac{[15]^2\langle 25\rangle^2}{[12]^2}(m_W^2 - m_t^2)(2m_W^2 + m_t^2). \tag{B.12}$$

Note the presence of squared spinor products, which cannot immediately be evaluated to form dot products. This is to be expected, given that $\tilde{\mathcal{M}}$ is not a Lorentz invariant quantity. To evaluate the quantities in eq. (B.12) one can parameterise 4-momenta in the center of mass frame of the incoming particles as follows:

$$p_1 = \left(\frac{\sqrt{s}}{2}, 0, 0, \frac{\sqrt{s}}{2}\right); \tag{B.13}$$

$$p_2 = \left(\frac{\sqrt{s}}{2}, 0, 0, -\frac{\sqrt{s}}{2}\right); \tag{B.14}$$

$$p_5 = (E, E\sin\theta\cos\phi, E\sin\theta\sin\phi, E\cos\theta). \tag{B.15}$$

Basis spinors satisfying the massless Dirac equation with conventional normalisation $u^\dagger(p_i)u(p_i) = 2p_i^0$ are (choosing arbitrary phases)

$$
u_-(p_5) = \begin{pmatrix} 0 \\ 0 \\ -\sqrt{E(1-\cos\theta)}e^{-i\phi} \\ \sqrt{E(1+\cos\theta)} \end{pmatrix} ; \quad
u_\lambda(p_1) = \begin{pmatrix} s^{\frac{1}{4}}\delta_{\lambda+} \\ 0 \\ 0 \\ s^{\frac{1}{4}}\delta_{\lambda-} \end{pmatrix} ; \quad
u_\lambda(p_2) = \begin{pmatrix} 0 \\ s^{\frac{1}{4}}\delta_{\lambda+} \\ s^{\frac{1}{4}}\delta_{\lambda-} \\ 0 \end{pmatrix} ,
$$

$$(B.16)$$

from which one finds

$$
\mathrm{Re}\left\{ \frac{\langle kp_2\rangle}{[kp_2]} \frac{[15]^2\langle 25\rangle^2}{[12]^2} \right\} = -\frac{(15)(25)}{s}[2\cos^2(\phi-\phi_{2k})-1], \qquad (B.17)
$$

with ϕ_{2k} the azimuthal relative angle between k and p_2. In the degenerate kinematics of the collinear limit, we may choose to absorb ϕ in a redefinition of ϕ_{2k}. Combining these results with eq. (B.12), and reinstating the colour, flux, average factors and coupling constants, gives finally

$$
\tilde{\mathcal{M}} = -\frac{g_s^2 g_W^2}{16 N s^2\, u_1^2 m_W^2}(2\cos^2\phi_{2k}-1)(m_W^2-m_t^2)(2m_W^2+m_t^2)(m_W^2 m_t^2 - ut). \quad (B.18)
$$

Note that this does indeed give zero contribution to the cross-section when integrated over the full domain of the azimuthal angle ϕ_{2k} relevant to the branching, as discussed above.

References

[1] R. Schwienhorst, talk given at the "Rencontres de Moriond EW 2008", La Thuile, 1-8 March 2008.

[2] V. M. Abazov *et al.* [D0 Collaboration], *Evidence for production of single top quarks*, [`arXiv:0803.0739 [hep-ex]`].

[3] S. Frixione and B. R. Webber, *Matching NLO QCD computations and parton shower simulations*, *JHEP* **06** (2002) 029 [`arXiv:hep-ph/0204244`].

[4] S. Frixione, P. Nason and B. R. Webber, *Matching NLO QCD and parton showers in heavy flavour production*, *JHEP* **08** (2003) 007 [`arXiv:hep-ph/0305252`].

[5] S. Frixione, E. Laenen, P. Motylinski and B. R. Webber, *Single-top production in MC@NLO*, *JHEP* **03** (2006) 092 [`arXiv:hep-ph/0512250`].

[6] S. Frixione, E. Laenen, P. Motylinski and B. R. Webber, *Angular correlations of lepton pairs from vector boson and top quark decays in Monte Carlo simulations*, *JHEP* **04** (2007) 081 [`arXiv:hep-ph/0702198`].

[7] T. M. P. Tait, *The tW⁻ mode of single top production*, *Phys. Rev.* **D61** (2000) 034001 [`arXiv:hep-ph/9909352`].

[8] A. S. Belyaev, E. E. Boos and L. V. Dudko, *Single top quark at future hadron colliders: Complete signal and background study*, Phys. Rev. D **59** (1999) 075001 [`arXiv:hep-ph/9806332`].

[9] B. P. Kersevan and I. Hinchliffe, *A consistent prescription for the production involving massive quarks in hadron collisions*, JHEP **0609** (2006) 033 [`arXiv:hep-ph/0603068`].

[10] S. Zhu, *Next-to-leading order QCD corrections to $bg \to tW^-$ at the CERN Large Hadron Collider*, *Phys. Lett.* **B524** (2002) 283–288.

[11] J. Campbell and F. Tramontano, *Next-to-leading order corrections to Wt production and decay*, *Nucl. Phys.* **B726** (2005) 109–130 [`arXiv:hep-ph/0506289`].

[12] Q. H. Cao, *Demonstration of One Cutoff Phase Space Slicing Method: Next-to-Leading Order QCD Corrections to the tW Associated Production in Hadron Collision*, [`arXiv:0801.1539 [hep-ph]`].

[13] M. Beccaria *et. al.*, *A complete one-loop description of associated tW production at lhc and a search for possible genuine supersymmetric effects*, [`arXiv:0705.3101 [hep-ph]`].

[14] N. Kauer and D. Zeppenfeld, *Finite-width effects in top quark production at hadron colliders*, *Phys. Rev.* **D65** (2002) 014021 [`arXiv:hep-ph/0107181`].

[15] S. Frixione, Z. Kunszt and A. Signer, *Three-jet cross sections to next-to-leading order*, *Nucl. Phys.* **B467** (1996) 399–442 [`arXiv:hep-ph/9512328`].

[16] S. Frixione, *A general approach to jet cross sections in QCD*, *Nucl. Phys.* **B507** (1997) 295–314 [`arXiv:hep-ph/9706545`].

[17] W. T. Giele, S. Keller and E. Laenen, *QCD corrections to W boson plus heavy quark production at the Tevatron*, *Phys. Lett.* **B372** (1996) 141–149 [`arXiv:hep-ph/9511449`].

[18] W. T. Giele and E. W. N. Glover, *Higher order corrections to jet cross-sections in e+ e- annihilation*, *Phys. Rev.* **D46** (1992) 1980–2010.

[19] W. T. Giele, E. W. N. Glover and D. A. Kosower, *Higher order corrections to jet cross-sections in hadron colliders*, *Nucl. Phys.* **B403** (1993) 633–670 [`arXiv:hep-ph/9302225`].

[20] S. Keller and E. Laenen, *Next-to-leading order cross-sections for tagged reactions*, *Phys. Rev.* **D59** (1999) 114004 [`arXiv:hep-ph/9812415`].

[21] G. Passarino and M. J. G. Veltman, *One Loop Corrections For $e^+ e^-$ Annihilation Into $\mu^+ \mu^-$ In The Weinberg Model*, Nucl. Phys. B **160** (1979) 151.

[22] T. Hahn, *Generating Feynman diagrams and amplitudes with FeynArts 3*, Comput. Phys. Commun. **140** (2001) 418 [arXiv:hep-ph/0012260].

[23] R. Mertig, M. Bohm and A. Denner, *FEYNCALC: Computer algebraic calculation of Feynman amplitudes*, Comput. Phys. Commun. **64** (1991) 345.

[24] J. A. M. Vermaseren, *New features of FORM*, [arXiv:math-ph/0010025].

[25] R. K. Ellis and G. Zanderighi, *Scalar one-loop integrals for QCD*, *JHEP* **0802** (2008) 002 [arXiv:0712.1851 [hep-ph]].

[26] J. Collins, F. Wilczek and A. Zee, *Low-energy manifestations of heavy particles: Application to the neutral current*, *Phys. Rev.* **D18** (1978) 242.

[27] F. Maltoni and T. Stelzer, *MadEvent: Automatic event generation with MadGraph*, JHEP **0302** (2003) 027 [arXiv:hep-ph/0208156].

[28] J. Alwall *et al.*, *MadGraph/MadEvent v4: The New Web Generation*, JHEP **0709** (2007) 028 [arXiv:0706.2334 [hep-ph]].

[29] G. Corcella *et al.*, *HERWIG 6: An event generator for hadron emission reactions with interfering gluons (including supersymmetric processes)*, JHEP **0101** (2001) 010 [arXiv:hep-ph/0011363].

[30] G. Corcella *et al.*, *HERWIG 6.5 release note*, [arXiv:hep-ph/0210213].

[31] A. Denner, S. Dittmaier, M. Roth and L. H. Wieders, *Electroweak corrections to charged-current $e^+ e^- \to 4$ fermion processes: Technical details and further results*, *Nucl. Phys.* **B724** (2005) 247 [arXiv:hep-ph/0505042].

[32] A. D. Martin, R. G. Roberts, W. J. Stirling and R. S. Thorne, *Uncertainties of predictions from parton distributions. i: Experimental errors. ((t))*, *Eur. Phys. J.* **C28** (2003) 455–473 [arXiv:hep-ph/0211080].

[33] E. Boos *et al.*, *Generic user process interface for event generators*, [arXiv:hep-ph/0109068].

[34] G. Leibbrandt, *Introduction to Noncovariant Gauges*, Rev. Mod. Phys. **59** (1987) 1067.

[35] A. Bassetto, G. Nardelli and R. Soldati, *Yang-Mills theories in algebraic noncovariant gauges: Canonical quantization and renormalization*, Singapore, Singapore: World Scientific (1991) 227 p

[36] F. James and M. Roos, *Minuit: A System For Function Minimization And Analysis Of The Parameter Errors And Correlations*, Comput. Phys. Commun. **10** (1975) 343.

[37] M. Cacciari, S. Frixione, M. M. Mangano, P. Nason and G. Ridolfi, *Updated predictions for the total production cross sections of top and of heavier quark pairs at the Tevatron and at the LHC* [arXiv:0804.2800 [hep-ph]].

[38] F. A. Berends, R. Kleiss, P. De Causmaecker, R. Gastmans and T. T. Wu, *Single Bremsstrahlung Processes In Gauge Theories*, Phys. Lett. B **103** (1981) 124.

[39] P. De Causmaecker, R. Gastmans, W. Troost and T. T. Wu, *Multiple Bremsstrahlung In Gauge Theories At High-Energies. 1. General Formalism For Quantum Electrodynamics*, Nucl. Phys. B **206** (1982) 53.

[40] Z. Xu, D. H. Zhang and L. Chang, *Helicity Amplitudes for Multiple Bremsstrahlung in Massless Nonabelian Gauge Theories*, Nucl. Phys. B **291** (1987) 392.

[41] R. Kleiss and W. J. Stirling, *Spinor Techniques For Calculating P Anti-P → W+- / Z0 + Jets*, Nucl. Phys. B **262** (1985) 235.

[42] J. F. Gunion and Z. Kunszt, *Improved Analytic Techniques For Tree Graph Calculations And The G G Q Anti-Q Lepton Anti-Lepton Subprocess*, Phys. Lett. B **161** (1985) 333.